Intelligent Sensing and Control for Autonomous Vehicle Following

by

Guang Lu

B.S.(Tsinghua University, Beijing, China) 1997
M.S.(University of Alabama) 1999

A dissertation submitted in partial satisfaction of the
requirements for the degree of
Doctor of Philosophy

in

Engineering-Mechanical Engineering

in the

GRADUATE DIVISION
of the
UNIVERSITY of CALIFORNIA at BERKELEY

Committee in charge:

Professor Masayoshi Tomizuka, Chair
Professor John Karl Hedrick
Professor Seth R. Sanders

Spring 2004

Intelligent Sensing and Control for Autonomous Vehicle Following

by

Guang Lu

Abstract

Intelligent Sensing and Control for Autonomous Vehicle Following

by

Guang Lu

Doctor of Philosophy in Engineering-Mechanical Engineering

University of California at Berkeley

Professor Masayoshi Tomizuka, Chair

This dissertation presents a new approach for automated vehicle steering control, i.e. the autonomous vehicle following approach. The goal of vehicle steering control is to achieve lane-keeping performance, i.e. to keep the vehicle close to the road centerline, by adjusting the steering angle at the tires in real time. Current vehicle steering control algorithms rely on road reference systems and appropriate on-board sensors to detect the vehicle's deviation from the road centerline. Therefore, these methods are referred to as road following algorithms. Autonomous vehicle following allows a vehicle to automatically follow its preceding vehicle based on real-time information of the relative distance between the two vehicles. If the leading vehicle tracks the road centerline reasonably well, this approach can achieve good lane-keeping performance of the controlled vehicle. The main benefit is that no road reference system is required for implementation of this new control scheme.

In this dissertation, the relative distance is measured by an on-board laser scanning radar (LIDAR) sensor. The sensing mechanism of LIDAR is based on the "Time of Flight" principle. The sensor emits laser beams to scan in the horizontal plane in search for the leading vehicle or any other reflective object in the environment. In each sampling period, the sensor returns 80 sets of measurements, most of which are caused by environmental clutter. A probabilistic data association based data processing method is used to extract the position information of the leading vehicle from the LIDAR measurements.

One issue in autonomous vehicle following is a propagation of errors from one vehicle to another. When errors increase in the upstream direction of a vehicle platoon, the platoon is string unstable. Analysis of string stability is performed, and inter-vehicle communication is suggested as a means to solve the string stability problem. Experimental results are used to show the effectiveness of the proposed solution.

Autonomous vehicle following may work as a back-up system for road following systems when the road following sensors are under partial failure. An integrated vehicle steering control scheme, which essentially combines the use of LIDAR and the remaining road following sensors, is introduced. The optimal combined use of LIDAR and a set of magnetometers mounted under the rear bumper of the test vehicle is considered. In the combined use of these two independent sensors, the interaction between the two system outputs is a major concern. Effects of

a disturbance associated with one sensor output on the other sensor output are investigated. This leads to solving the problem of minimizing the interaction between the two system outputs. The solution is verified by both simulations and real-time testing.

Professor Masayoshi Tomizuka
Dissertation Committee Chair

To my loving family

Contents

List of Figures

List of Tables

Acknowledgements

The first person I would like to thank is my research advisor, Professor Masayoshi Tomizuka, for his consistent support, guidance, and encouragement in achieving this dissertation. Professor Tomizuka's warm-heartedness, understanding, and patience are unbelievable, and I will cherish, for ever, my experience of working as one of his graduate students.

I would like to thank Professor John Karl Hedrick and Professor Seth R. Sanders for serving as members of my dissertation committee.

I would like to thank many PATH researchers and staff, Dan Empey, David Nelson, Anouck Girard, Adam Howell, Han-Shue Tan, Paul Kretz, Thang Lian, Bart Duncil, Xiao-Yun Lu, Ching-Yao Chan, Benedicte Bougler, Scott Johnston, and Stephen Spry. Without their help, I could not have made my experiments possible.

I would like to thank all my fellow graduate students in Etcheverry 2103 for sharing their knowledge, experience, and culture with me. Especially, I would like to thank Sandipan Mishra for proofreading this dissertation and Shianglung Koo for spending his time helping me in my experiments. I would like to thank all other current and past group members, Tesheng, Soo, Ahmed, Jihua, Chun-chih, Shang-Chen, Erwin, Ye, Kun, Jiagen, Hector, Jengyu, Ryan, Craig, and Iakovos, for being supportive and cooperative colleagues.

I would like to thank my parents Weiliang Lu and Guiting Zhou, my sister

Jing Lu and her husband Chengmin Wang, my brother Dr.Hong Lu and his wife Dr.Yan Li, and my wife Fang Li for their love, support, and encouragement.

This work was supported by the California Department of Transportation (CalTrans) under PATH TO4204. I would like to thank Nissan Motor Corporation for providing the laser scanning radar sensor for this research.

Chapter 1

Introduction

Intelligent vehicle control has been actively studied in recent years. An important topic in this research field is steering control. In this chapter, two different approaches for vehicle steering control are introduced. The conventional road-following approach relies on on-board sensors to measure the vehicle's lateral deviation from the road centerline, which in general requires road infrastructure. The new approach, autonomous vehicle following, does not need any road infrastructure, and hence it is easy to implement. A qualitative analysis reveals that this approach may have a potential error propagation problem. Another key problem in autonomous vehicle following is the data processing issue for the sensor outputs. The integrated use of the two approaches becomes useful for certain scenarios. These considerations motivate the research on intelligent sensing and control algorithms for autonomous vehicle following. The objectives and contributions of

this dissertation are stated toward the end of this chapter, which is followed by an outline of the dissertation.

1.1 Vehicle Steering Control

The goal of automated vehicle steering control is to calculate and actuate correct steering angle at the tires, as the control input, to generate desired tire force through the road-tire interaction process. The tire force steers the vehicle in the desired direction to regulate the vehicle's lateral deviation from the road centerline, which is referred to as the absolute deviation. Hence, vehicle steering control is also called lane-keeping control or vehicle lateral control. In most of the current steering control schemes, the absolute deviation is measured directly by on-board sensors and used as a feedback signal. These control schemes constitute a road following approach. The control algorithms described in (5)(12)(17)(27) use on-board vision cameras, and the absolute deviation is obtained by extracting the lane markers in detected images through an image processing procedure. Instead, magnetometers are used in (6)(14)(32)(33) to measure the vehicle's absolute deviation by detecting the magnetic field generated by the magnetic markers buried under the road centerline. The steering controller then determines the desired steering command in order to keep the vehicle inside the lane. This control scheme is shown in Fig.1.1. Clearly, the road following approach relies on the road reference system on the infrastructure side, e.g. lane markers and magnetic

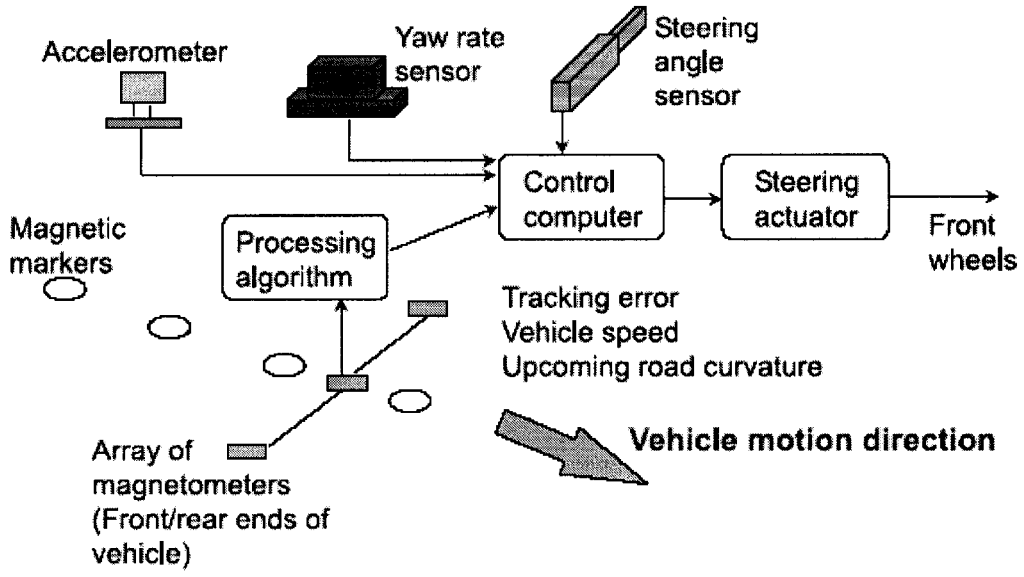

Figure 1.1: Magnetometer-based vehicle steering control architecture

markers.

1.2 Autonomous Vehicle Following

In recent years, some researchers (23)(10)(11) have investigated a different approach to vehicle steering control. Instead of measuring the absolute deviation of the controlled vehicle, the on-board sensors detect the vehicle's relative position with respect to a leading vehicle, referred to as the relative deviation. The following vehicle is then controlled to follow the leading vehicle based on the relative deviation. Compared to the traditional steering control approach, this control scheme, referred to as autonomous vehicle following control, requires no road reference system, neither lane markers nor magnetic markers. Automated steering

control can be enabled whenever the controlled vehicle has a preceding vehicle that tracks the road centerline. Autonomous vehicle following may work as a driver assistance system, similar to today's cruise control systems except that the system assists a driver in steering instead of speed control. It can also be combined with the cruise control system to achieve fully automated control of a vehicle. Such a system is called the electrical tow-bar (9)(31). Detecting the relative deviation is a key in developing such a control system. Environmental clutter may cause severe noise on the sensor measurements. Therefore, data processing algorithms have to be implemented to effectively track the position of the lead vehicle based on sensor measurements in real time.

1.3 Error Propagation In Autonomous Vehicle Following

Since the control algorithm in autonomous vehicle following is based on the vehicle's relative deviation from the leading vehicle, the lane-keeping performance of the following vehicle depends on the behavior of the leading vehicle. If the leading vehicle tracks the road centerline badly, so will the following vehicle, and in general with even worsened performance. The lead and the following vehicles now form an inter-connected system, and the tracking error of the lead vehicle is passed on to the following vehicle. This aspect of the autonomous following

Figure 1.2: A platoon of vehicles under automated steering control

causes a severe string stability problem, when the algorithm is applied to a platoon of many vehicles. An example of vehicle platooning is shown in Fig.1.2. String stability is concerned with propagation of tracking errors in the upstream direction of the platoon, i.e. from leading to following vehicles. A platoon may be string unstable even if the control system of each vehicle is stable. It also places significant limitations on the performance of autonomous following control even for small groups of vehicles. This problem for autonomous following has not been analyzed in the previous research.

It is the inter-connected feature that causes the propagation of tracking errors in the platoon. To improve the vehicle tracking performance, it is intuitively helpful to weaken or cut the coupling between any two adjacent vehicles so that the tracking performance of one vehicle does not depend on that of the other. Besides the relative deviation, information on how well the preceding vehicle follows the

road may also be useful for the lane-keeping control of the following vehicle. When the leading vehicle follows the road badly, the following vehicle can respond in an intelligent way and may still achieve good tracking performance. Hence, inter-vehicle communication becomes important in autonomous vehicle following control in terms of transmitting measurements of the absolute deviation of a leading vehicle to its following vehicles. Using inter-vehicle communication, a leading vehicle in the platoon, which can measure its absolute deviation (e.g. by the means of GPS or vision cameras), communicates its measurements to the following vehicles. The control algorithm of a following vehicle calculates its steering input based on both the relative deviation from the leading vehicle and the communicated information to keep the vehicle in the lane.

1.4 Integrated Steering Control

Autonomous vehicle following control may become helpful to road following systems when the road following sensors fail. It may work as a back-up system to replace the road following system when all the road following sensors stop functioning. For the magnet-magnetometer based approach, back-up systems are studied to deal with partial failure of magnetometers. Currently there are two sets of magnetometers on-board each vehicle, one under the front bumper and the other under the rear bumper. Previous research indicates that the front magnetometers are critical for vehicle lateral control. More precisely, if the front magnetometers fail,

a right-half-plane zero appears on the pole-zero map of the input-output dynamics from the front wheel steering angle to the lateral error at the rear bumper, which may deteriorate the performance of the lane-keeping system. In this case, the desired vehicle performance may be achieved by combining the rear magnetometers with the autonomous vehicle following sensor. The magnetometer measurements can also help to reduce the dependence of the following vehicle on the lead vehicle, and hence reduce the tracking errors. Under this integrated control scheme, the controlled plant, i.e. the vehicle, becomes a Single Input, Two Output (SITO) system: the front wheel steering angle is the input and the rear magnetometers and LIDAR define the two outputs. In the closed-loop structure, disturbances in one system output may have strong effects on the other output. Such a problem becomes a significant concern in the design of the integrated control scheme, since the LIDAR measurements are associated with strong disturbance, which is the unknown dynamics of the leading vehicle.

1.5 Objectives and Contributions

The main objectives of this dissertation research are as follows

- to develop an autonomous vehicle following control system, including sensing and control algorithms, and to investigate the system's lane-keeping performance in a road-fixed coordinate frame

- to analyze the error propagation problem in autonomous vehicle following and to search for possible solutions

- to conduct research on the possibility and effects for integrated use of both the road following and autonomous vehicle following approaches

There are three main contributions in this dissertation:

- A probabilistic data association method is proposed for processing the sensor measurements. Information on the vehicle's relative distance from the preceding vehicle is extracted from the measurements regardless of surrounding environmental clutter. With such a data processing algorithm, the on-board sensor effectively tracks the position of the preceding vehicle in real time.

- The autonomous vehicle following problem is formulated as an inter-connected system, and the coupling between adjacent vehicles is investigated. The string stability of the entire system is then analyzed, and an inter-vehicle communication based solution is proposed.

- The integrated control scheme is formulated as the design problem for a Single Input Two Outputs (SITO) plant, and an optimal method for combining the use of two different types of sensors is proposed by minimizing the interaction between the sensor outputs such that the disturbance associated with any one sensor output has minimum effects on the other sensor output.

1.6 Outline

Chapter 2 discusses modeling of the vehicle lateral dynamics. A simplified vehicle model is introduced, and the effects of the sensor locations and vehicle velocities are analyzed. The output of the autonomous vehicle following sensor is described to fit in to this simplified model.

Chapter 3 describes the working scheme of the sensor and sensor data processing algorithm used in autonomous vehicle following. A laser scanning radar (LIDAR) sensor is used to detect the relative distance between the controlled vehicle and the preceding vehicle. Its measurement mechanism is based on the "Time of Flight" principle, where the distance equals to the product of travel time and speed of light. In each sampling period, the sensor scans in the horizontal plane for 80 steps searching for the target. Hence information about the position of the target has to be extracted from the 80 sensor measurements in real time. This is achieved by a data processing algorithm based on probabilistic data association.

Chapter 4 presents the LIDAR-based autonomous vehicle following control algorithms, and evaluates system performance in the magnetic reference system in real-time experiments. The error propagation problem is investigated in simulations, and the string stability problem is analyzed by formulating the problem as an inter-connected system. Inter-vehicle communication is proposed as a practical solution to this problem, and its performance is validated by experiments.

Chapter 5 investigates the integrated control with combined use of both LI-

DAR and magnetometers. The measurements of the two different types of sensors are combined optimally for control in the sense that disturbance associated with each sensor output has minimum effect on the other sensor output. Experimental results are presented.

Chapter 6 summarizes the background, motivations, objectives, algorithms, analysis, simulations, and experimental results presented in this dissertation. The effectiveness of the proposed methods for solving technical problems in autonomous vehicle following is evaluated, and some future work is suggested.

Chapter 2

Vehicle Lateral Dynamics

Vehicle lateral dynamics have been studied since late 1950's. Segel (1956) (28) developed a three-degree-of freedom vehicle model to describe the vehicle directional responses, which includes the yaw, lateral and roll motions. Vehicle models with more degree-of-freedoms were developed by Lugner(1977)(22), and Peng and Tomizuka (1990)(26). In most cases, a simplified model (bicycle model) provides sufficient accuracy in the design of control laws. Previous research work also indicates the significance of sensor locations in the design of control laws for automated steering. In this chapter, first the bicycle model is introduced. This is followed by the analysis of the model for different sensor locations. Finally, the effect of vehicle following sensor is modeled to fit into the above framework.

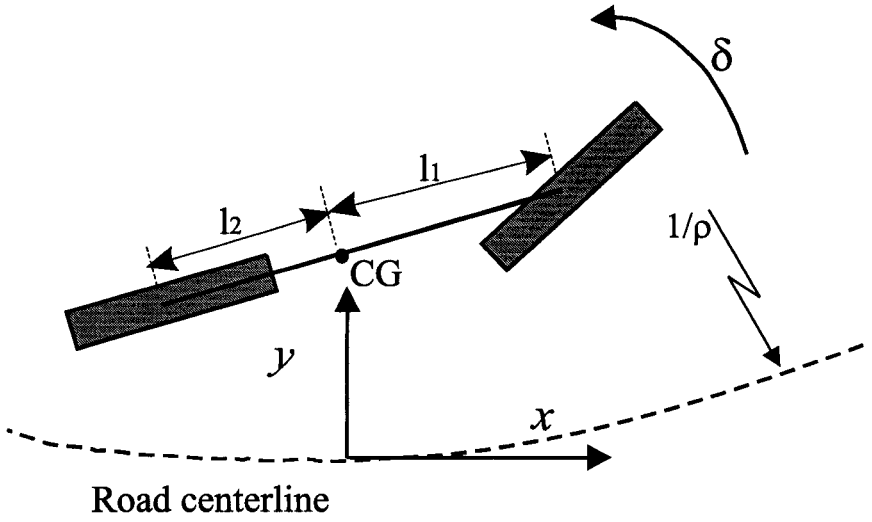

Figure 2.1: Bycicle model

2.1 Bicycle Model

For simplicity, this dissertation considers only front-wheel-steered vehicles. For a single vehicle, the bicycle model is used for analysis and design of control laws. The model is depicted in Fig.2.1, where CG denotes the center of gravity of the vehicle and other variables and parameters are defined later. The lateral force generated through the road-tire interaction applies to the vehicle, and causes lateral motion. The model is based on the following assumptions(14).

- Roll, pitch or bounce motions are negligible.
- The relative yaw between vehicle and the road is small.
- The steering angle is small.
- The tire lateral force varies linearly with the slip angle.

Based on the above assumptions, the bicycle model in the road reference frame is:

$$m\ddot{y} = -m\dot{\epsilon}\dot{x} - \frac{C_{\alpha_r}(\dot{y} - \dot{\epsilon}l_2)}{\dot{x}} - \frac{C_{\alpha_f}(\dot{y} + \dot{\epsilon}l_1)}{\dot{x}} + C_{\alpha_f} \tag{2.1}$$

$$I_z\ddot{\epsilon} = l_2\frac{C_{\alpha_r}(\dot{y} - \dot{\epsilon}l_2)}{\dot{x}} - l_1\frac{C_{\alpha_f}(\dot{y} + \dot{\epsilon}l_1)}{\dot{x}} + l_1C_{\alpha_f} \tag{2.2}$$

where $\dot{x}$ and $\dot{y}$ are the components of the vehicle velocity along longitudinal and lateral principle axis of the vehicle body, $\dot{\epsilon}$ is the yaw rate, m and I_z are the mass and the yaw moment of inertia, respectively, l_1 and l_2 are respectively distances of the front and rear axle from CG, C_{α_f} and C_{α_r} represent the front and rear tire cornering stiffness, respectively, and δ is the steering angle. Equations 2.1 and 2.2 can also be written as,

$$\ddot{y}_s = f_1 + b_1\delta \tag{2.3}$$

$$\begin{aligned}\ddot{\epsilon}_r = &\frac{l_1C_{\alpha_f} - l_2C_{\alpha_r}}{I_z\dot{x}}\dot{y}_s + \frac{l_1C_{\alpha_f} - l_2C_{\alpha_r}}{I_z}\epsilon_r + \frac{C_{\alpha_f}l_1}{I_z}\delta - \\ &\frac{C_{\alpha_f}({l_1}^2 - l_1d_s) + C_{\alpha_r}({l_2}^2 + l_2d_s)}{I_z\dot{x}}\dot{\epsilon}_r - \frac{C_{\alpha_f}{l_1}^2 + C_{\alpha_r}{l_2}^2}{I_z\dot{x}}\dot{\epsilon}_d\end{aligned} \tag{2.4}$$

where d_s is the distance between the measurement point and the vehicle CG, y_s represents the vehicle lateral error at the measurement point (either real or virtual), ϵ_r is the relative yaw angle, and f_1 and b_1 are given as follows.

$$f_1 = -\frac{\phi_1 + \phi_2}{\dot{x}}\dot{y}_s + (\phi_1 + \phi_2)\epsilon_r + \frac{\phi_1(d_s - l_1) + \phi_2(d_s + l_2)}{\dot{x}}\dot{\epsilon}_r + \frac{\phi_2l_2 - \phi_1l_1 - \dot{x}^2}{\dot{x}}\dot{\epsilon}_d \tag{2.5}$$

$$b_1 = \phi_1 \tag{2.6}$$

$$\phi_1 = C_{\alpha_f}(\frac{1}{m} + \frac{l_1d_s}{I_z}) \tag{2.7}$$

$$\phi_2 = C_{\alpha r}(\frac{1}{m} - \frac{l_2 d_s}{I_z}) \tag{2.8}$$

The state-space-form representation of these equations is

$$\dot{\xi} = A\xi + B\delta + W\rho \tag{2.9}$$

where

$$\xi = \begin{pmatrix} y_s & \dot{y}_s & \epsilon & \dot{\epsilon} \end{pmatrix}^T \tag{2.10}$$

$$A = \begin{pmatrix} 0 & 1 & 0 & 0 \\ 0 & -\frac{a_{11}}{\dot{x}} & a_{11} & \frac{a_{12}}{\dot{x}} \\ 0 & 0 & 0 & 1 \\ 0 & -\frac{a_{41}}{\dot{x}} & a_{41} & \frac{a_{42}}{\dot{x}} \end{pmatrix} \tag{2.11}$$

$$B = \begin{pmatrix} 0 \\ b_{21} \\ 0 \\ b_{41} \end{pmatrix} \tag{2.12}$$

$$W = \begin{pmatrix} 0 \\ w_{21} \\ 0 \\ w_{41} \end{pmatrix} \tag{2.13}$$

$$a_{11} = (\phi_1 + \phi_2), a_{12} = \phi_1(d_s - l_1) + \phi_2(d_s + l_2) \tag{2.14}$$

$$a_{41} = \frac{l_1 C_{\alpha_f} - l_2 C_{\alpha_r}}{I_z} \tag{2.15}$$

Table 2.1: Vehicle Parameters

Symbols	Physical Meaning	Value
m	mass	$1485kg$
L	relative longitudinal distance between vehicles	$8m$
h_1	distance of front bumper to CG	$2.7m$
h_2	distance of rear bumper to CG	$2.1m$
d_s	distance of sensor location to CG	
	distance between vehicles	
I_z	yaw moment of inertia	$2872kg/m^2$
C_{α_f}	front wheel cornering stiffness	$42000N/rad$
C_{α_r}	rear wheel cornering stiffness	$42000N/rad$
l_1	distance between front wheel and the CG	$1.1m$
l_2	distance between rear wheel and the CG	$1.58m$

$$a_{42} = \frac{l_1 C_{\alpha_f}(d_s - l_1) + l_2 C_{\alpha_r}(d_s + l_2)}{I_z} \tag{2.16}$$

$$b_{21} = \phi_1, b_{41} = \frac{l_1 C\alpha_f}{I_z} \tag{2.17}$$

$$w_{21} = -\frac{{l_1}^2 C_{\alpha_f} + {l_2}^2 C_{\alpha_r}}{I_z} \tag{2.18}$$

$$w_{41} = \phi_2 l_2 - \phi_1 l_1 - \dot{x}^2 \tag{2.19}$$

and $\rho = \frac{\dot{\epsilon_d}}{\dot{x}}$ is the road curvature, which is treated as a disturbance in most lateral controller designs. The physical meaning and values of the symbols are listed in Table 2.1.

In the above description, the steering angle δ in the state-space equation is the control input. The control algorithm calculates the steering angle to generate the desired lateral force and hence the desired lateral motion so that the lateral deviation of the vehicle is regulated. The road curvature ρ is considered small for highway applications, and it is treated as disturbance in system analysis and controller design.

2.2 Sensor Location Analysis

Note that the lateral deviation can be measured at any point of the vehicle, not necessarily at the vehicle's CG. Assuming that the sensor is located at distance d_s ahead of the vehicle's CG, the sensor output is

$$y_s = \begin{pmatrix} 1 & 0 & d_s & 0 \end{pmatrix} \xi \tag{2.20}$$

The position of the sensor determines the location of the system zeros of the transfer function from the steering input to the sensor output. At a fixed vehicle speed, the amount of phase lead increases as d_s increases (see Fig.2.2), which makes the system easy to stabilize. Because of this property, the steering control algorithms described in (13)(14)(25) employ a geometric look-ahead scheme, where the lateral error at some distance ahead of the vehicle CG, i.e. at a large d_s, is geometrically constructed from two sets of magnetometers (mounted under the front and rear bumpers) and used as the feedback signal. As shown in Fig.2.3, the

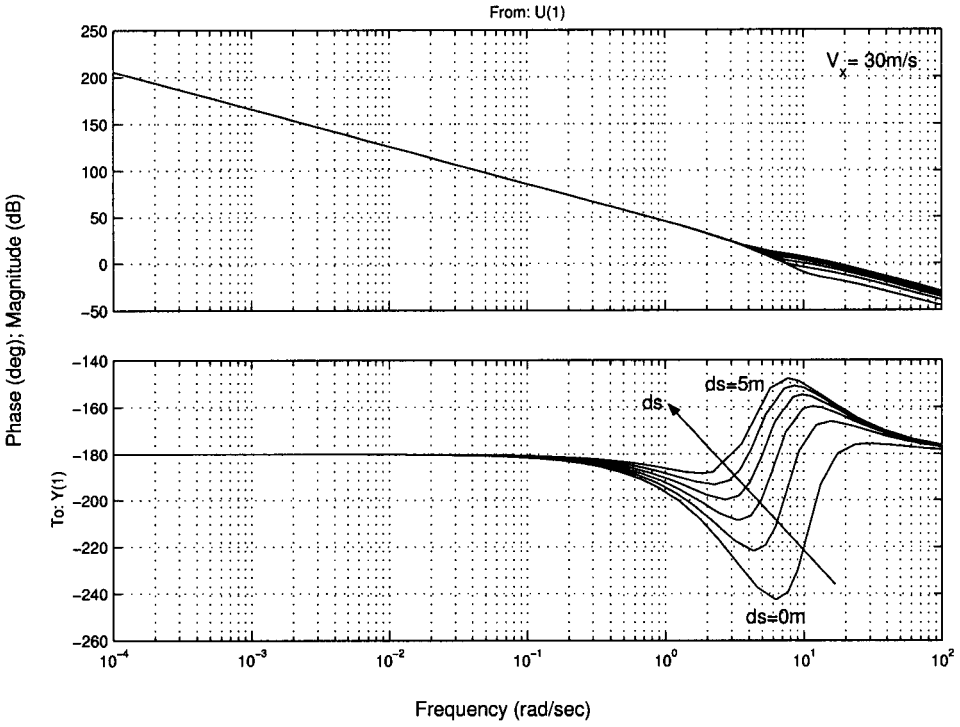

Figure 2.2: Bode plot of the transfer function from the steering input to the sensor output obtained at different locations)

virtual lateral error y_{vs} can be calculated from the front and rear magnetometer measurements (denoted by y_{fs} and y_{rs} respectively) by

$$y_{vs} = \frac{(h_2 + d_s)y_{fs} + (h_1 - d_s)y_{rs}}{h_1 + h_2} \tag{2.21}$$

The control objective is to minimize the virtual lateral error. In other words, the control system using geometric look-ahead scheme is trying to minimize the lateral error at some distance ahead of the vehicle.

In the case when one set of the magnetometers fails, the look-ahead distance in the above geometric scheme decreases to certain fixed values. This is based on the assumption that the fault detection process has been carried out and

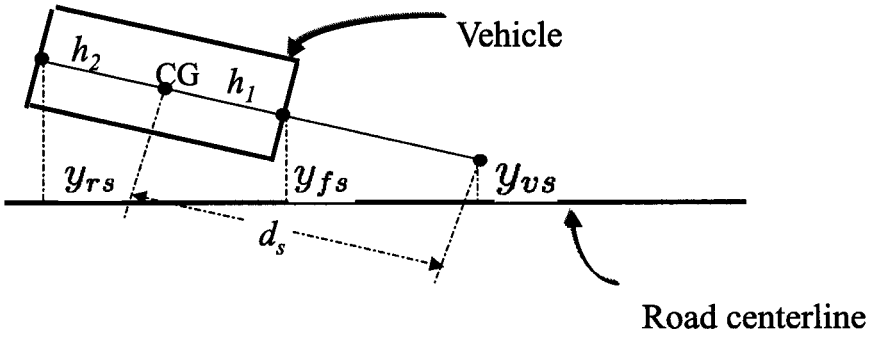

Figure 2.3: Geometric look-ahead scheme

the outputs of all failed magnetometers have been set to zero. When the front magnetometers fail, only the lateral error measured by the rear magnetometers is available to the control system, and the look-ahead distance d_s decreases to $-h_2$ (h_2 is the distance from the CG to the rear bumper). Similarly, under fault in rear magnetometers, the look-ahead distance decreases to h_1 (the distance from the CG to the front bumper). In the second case, the look-ahead distance is small and the phase lead in the system may not be adequate; in the first case, the look-ahead distance is negative, and it is not even "look-ahead" any more. Figures 2.4 and 2.5 show the frequency responses from the steering input δ to the lateral error measured by the front magnetometers y_{sf} and by the rear magnetometers y_{sr} when the longitudinal velocity is $30m/s$. The decreased phase lead makes the controller design difficult, especially for the case with front magnetometer failure. This problem will be revisited in Chapter 5.

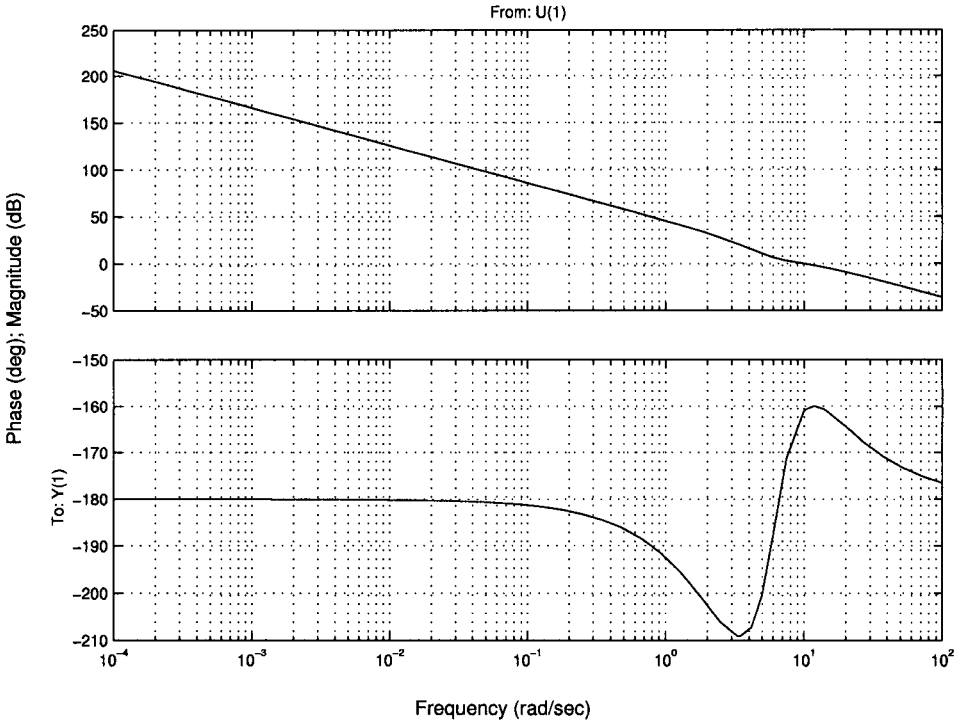

Figure 2.4: Bode plot of the transfer function from the steering input to front magnetometer output

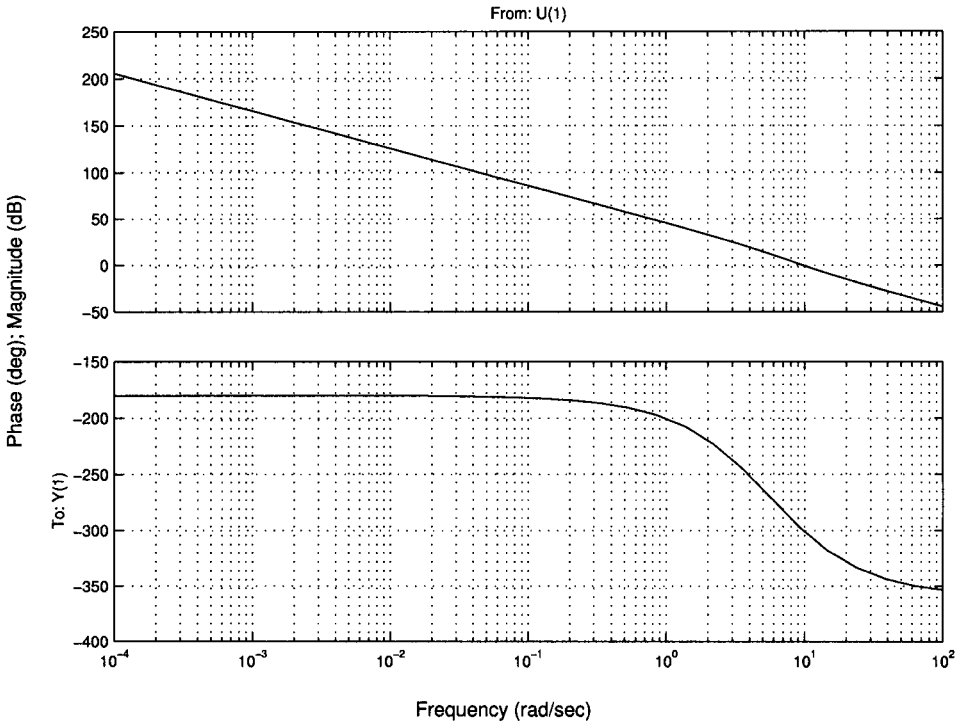

Figure 2.5: Bode plot of the transfer function from the steering input to rear magnetometer output

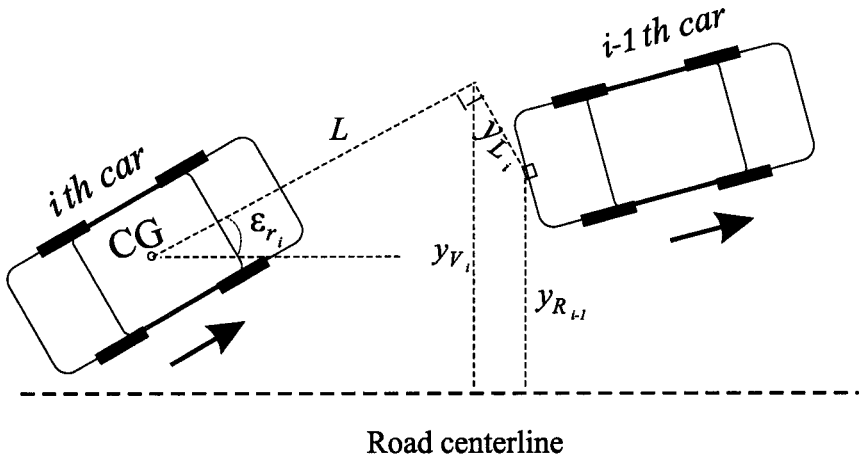

Figure 2.6: Autonomous vehicle following measurement scheme

2.3 Sensing for Autonomous Vehicle Following

Autonomous vehicle following relies on some on-board sensors to measure the relative distance from the controlled vehicle to the preceding vehicle. To mathematically express the sensor measurements, a few assumptions are used. First, since this research is intended for highway applications, only small road curvatures (less than $\frac{1}{800m}$) are considered. The road curvature is hence neglected in the distance between the two vehicles.

As shown in Fig.2.6, L and y_{L_i} denote the longitudinal and lateral distance, between the $(i-1)$th and ith vehicles, measured by the sensor. y_{Ri-1} represents the absolute deviation of the $(i-1)$th vehicle at the position where the target is placed. Let y_{Vi} denote the virtual absolute deviation of the ith vehicle at the distance L ahead of the vehicle CG. Then,

$$y_{Vi} = C_2 \xi_i \tag{2.22}$$

and

$$y_{Ri-1} = C_1 \xi_{i-1} \tag{2.23}$$

where ξ_i denotes the state vector of the ith vehicle, and

$$C_2 = \begin{pmatrix} 1 & 0 & L & 0 \end{pmatrix} \tag{2.24}$$

$$C_1 = \begin{pmatrix} 1 & 0 & -h_2 & 0 \end{pmatrix} \tag{2.25}$$

The lateral measurement by the autonomous vehicle following sensor of the ith vehicle can be represented as

$$y_{Li} = \frac{(y_{Vi} - y_{Ri-1})}{cos\ \epsilon_{ri}} \tag{2.26}$$

where ϵ_{ri} is the yaw angle of the ith vehicle relative to the road centerline. It is further assumed that ϵ_{ri} is small. Then,

$$y_{Li} \approx (y_{Vi} - y_{Ri-1}) \tag{2.27}$$

The above equations show that the measurement by the autonomous vehicle following sensor is essentially a look-ahead measurement, i.e. the sensor measures the lateral deviation at a point with distance L ahead of the vehicle's CG. Thus, using the sensor measurement as the feedback signal to the controller automatically provides similar benefits to those of the virtual look-ahead scheme in (13)(14).

It is also clear from the above equations that the platoon that consists of the lead and the following vehicles becomes an interconnected system. For this interconnected system, stability of each system component, i.e. each vehicle, cannot

guarantee the stability of the entire system because the system components are not independent. Instead, string stability needs to be considered. Further discussion of string stability will be given in Chapter 4.

Chapter 3

LIDAR and Data Processing

In autonomous vehicle following, one vehicle is automatically steered to follow the preceding vehicle based on information about the relative distance between the vehicles. For this dissertation research, information of the relative distance is obtained by an on-board laser scanning radar (LIDAR) sensor. The sensor detects the target by sending out laser beams and receiving the beams reflected by the target. The sensor measurements may encounter environmental clutter caused by the numerous reflective objects on the roadway. A data processing algorithm called probabilistic data association method is used to process the sensor measurements, i.e. to extract information of the relative distance. This chapter starts with the description of the sensor, and then the data processing algorithm is presented.

3.1 Laser Scanning Radar Sensor (LIDAR)

For autonomous vehicle following, a laser scanning radar sensor (LIDAR) shown in Figs.3.1 and 3.2 has been used to measure the relative distance from the leading vehicle to the following vehicle. As shown in Fig.3.3, the LIDAR sensor consists of a laser diode, a scanning mechanism, and a receiver. The laser diode emits laser beams to the roadway. The scanning mechanism is a rotating prism, and it makes the laser beams scan in the horizontal plane. If the laser beams hit any reflective object on the roadway, they will bounce back. The reflected laser beams can be detected by the built-in receiver. The distance from the sensor to the object is measured by the "Time of Flight" (TOF) principle, which says:

$$s = c \cdot T \tag{3.1}$$

where s is the distance from the sensor to the target, T is the flight time of the laser beam before it reaches the target, and c is the speed of the light, which is 2.976×10^8 m/s. Since the laser beams scan in the horizontal plane with constant steps, the orientation of the object can also be measured by counting the number of the scanning steps. Hence, the position of an object is uniquely defined in two dimensional space. The measured position is written in polar coordinates, and can be later converted to Cartesian. In autonomous vehicle following, a target with a reflective surface is fixed on the rear bumper of the leading vehicle, and a LIDAR sensor is installed on the following vehicle; therefore, the relative distance between

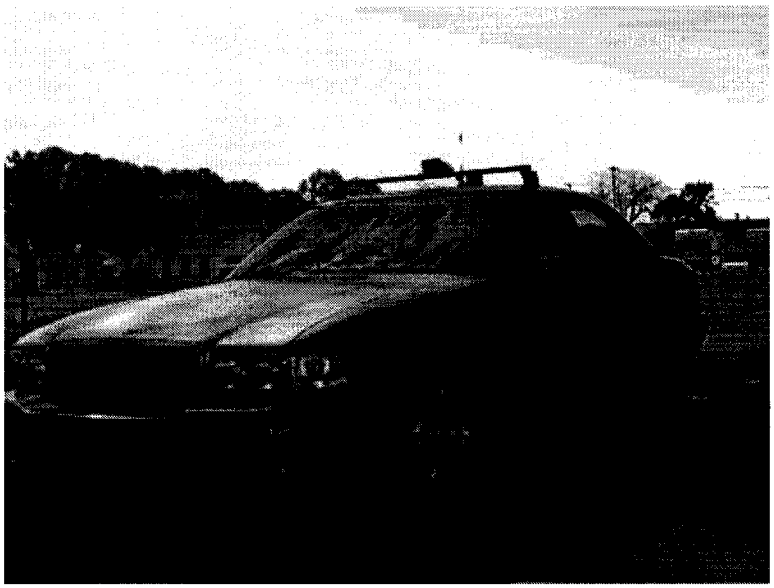

Figure 3.1: LIDAR mounted on the top of the vehicle

the two test vehicles can be measured.

The laser beam emitted by the LIDAR sensor used in this study scans horizontally 12^o in 80 equal steps for every $100msec$. At each step, the LIDAR sensor measures the distance and angular position of the object that reflects the laser beams along with the intensity of the reflection. The intensity information is shown in the form of an integer varying from 0 to 31. The specification of the LIDAR sensor is shown in Table 3.1. If the longitudinal distance between the two vehicles is $10m$, the width of the scanning area is about $2m$ with the resolution of $0.025m$. A set of 162-byte is transmitted every $100ms$ cycle through the serial port. The data specification is listed in Table 3.2.

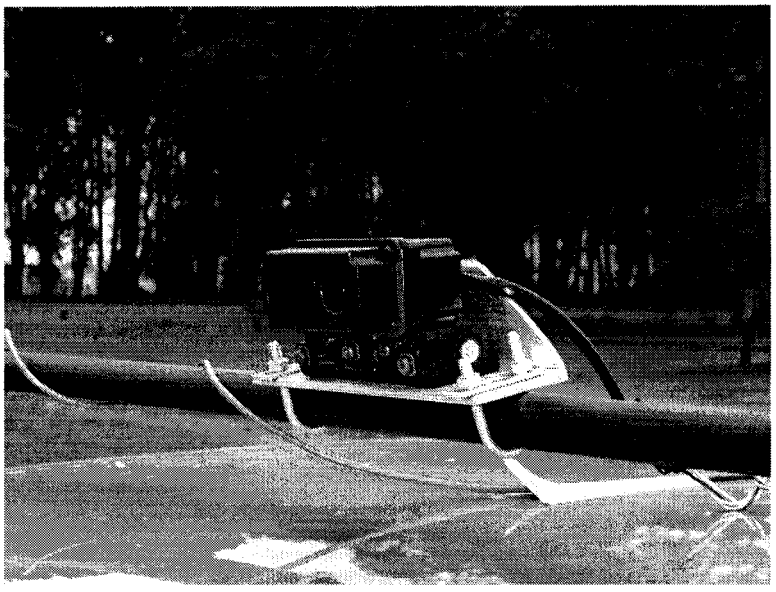

Figure 3.2: LIDAR: a closer look

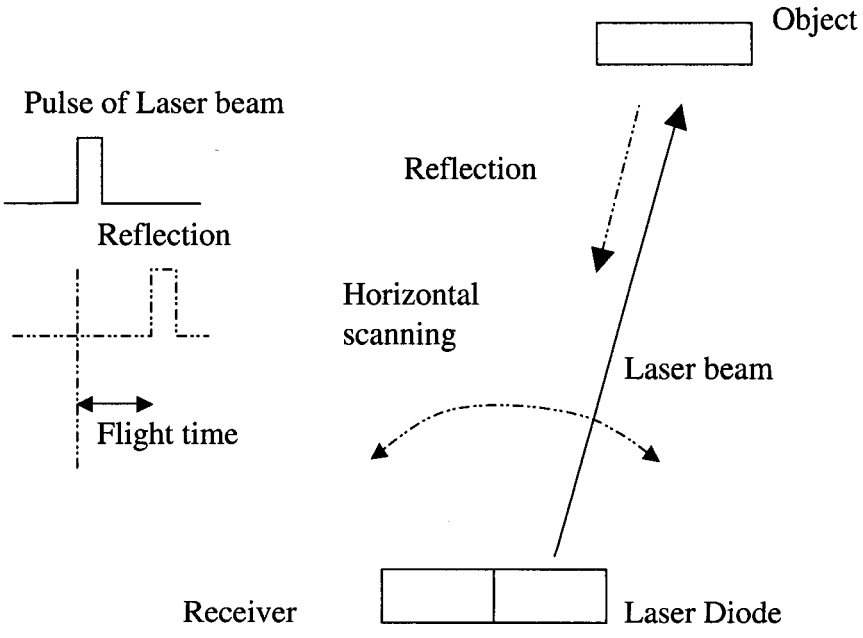

Figure 3.3: LIDAR working scheme

Table 3.1: LIDAR Specification

class of laser beam	class 1
wave length	$800nm$ (infrared)
distance resolution	$0.15m$
number of scanning steps	80
scanning angle of each step	0.15^o
scanning range of angle	12^o
vertical beam width	4^o(laser beam is narrowly focused in horizontal direction)

Table 3.2: Data Specification for LIDAR

Serial Communication Specification	Value
speed	$38400bps$
start bit	1 bit
data length	8 bits
parity	even
stop bit	1 bit

3.2 Probabilistic Data Association

When the laser beam scans, it detects anything reflective on the roadway. Since there are numerous reflective objects and surfaces in the environment, the LIDAR sensor returns one set of measurements in every scanning step. For each sampling period, the LIDAR sensor returns 80 sets of measurements, most of which are not related to the desired target. Extraction of the useful information about the real position of the desired target from the sensor measurements is a key research issue in autonomous vehicle following.

At the first thought, picking one measurement that has the strongest intensity

value seems to be a natural idea. However, two main concerns arise about this method. First, the intensity data is quite rough, because it is an integer varying from 0 to 31. Hence it is not practical to rely on the intensity data to make the decision. Second, picking only one measurement is of high risk, because the algorithm is very likely to keep tracking a wrong target if a wrong selection is made at some sampling point in the past.

To determine the actual position of the target of interest, a probability data association method proposed by Bar-Shalom(2) has been applied to process the LIDAR measurements. The fundamental idea of the data processing algorithm is to combine all the validated measured data according to their probabilities of being the correct measurement to update a Kalman filter. The data points that are more likely to be the correct measurements receive higher weights in the algorithm than other data points. This is based on the assumption that all measurements are normally distributed around a predicted point. Details of this algorithm are described in the next section.

3.3 LIDAR Data Processing Algorithm

The LIDAR data processing algorithm based on probabilistic data association is described as follows. First, the kinematic target motion is described as

$$x[k+1] = A_s x[k] + B_{ws} w[k] \tag{3.2}$$

where $x[k]$ is the state vector consisting of the position and velocity of the target described in Cartesian coordinates,

$$x[k] = [x_{target}, \dot{x}_{target}, y_{target}, \dot{y}_{target}]^T, \tag{3.3}$$

$w[k]$ consists of the normally distributed, zero mean, white process noise in x and y directions,

$$w[k] = \begin{pmatrix} w_x[k] \\ w_y[k] \end{pmatrix} \tag{3.4}$$

$$A_s = \begin{pmatrix} 1 & T_s & 0 & 0 \\ 0 & 1 & 0 & 0 \\ 0 & 0 & 1 & T_s \\ 0 & 0 & 0 & 1 \end{pmatrix} \tag{3.5}$$

$$B_{ws} = \begin{pmatrix} \frac{T_s^2}{2} & 0 \\ T_s & 0 \\ 0 & \frac{T_s^2}{2} \\ 0 & T_s \end{pmatrix} \tag{3.6}$$

and T_s is the sampling time of LIDAR sensor. Although LIDAR measurements arrive in polar coordinates, they are converted to Cartesian. Accordingly, the measurement model is given by

$$z[k] = H_s x[k] + v[k] \tag{3.7}$$

where

$$H_s = \begin{pmatrix} 1 & 0 & 0 & 0 \\ 0 & 0 & 1 & 0 \end{pmatrix}, \tag{3.8}$$

and $v[k]$ consists of the zero mean, white, Gaussian measurement noises in x and y directions,

$$v[k] = \begin{pmatrix} v_x[k] \\ v_y[k] \end{pmatrix}. \tag{3.9}$$

$x[0]$, $w[k]$, and $v[k]$ are independent. Based on the past observations, the algorithm predicts the state of the target for the current time step. The prediction equations are

$$\hat{x}[k|k-1] = A_s\hat{x}[k-1|k-1] \tag{3.10}$$

$$\hat{z}[k|k-1] = H_s\hat{x}[k|k-1]. \tag{3.11}$$

The data processing algorithm now has to estimate the target state according to the current measurements. At time index k, LIDAR returns 80 measurements, denoted by $\{z_i[k]\}_{i=1}^{80}$. For estimation of the target position, only those measurements that fall into a validation region, which will be explained later, are considered. The best estimate of the target's state is the conditional mean based upon all the observations with some nonzero probability originating from the target. For simplicity, the probability density of the target's state conditioned upon the past observations is assumed normal with mean $\hat{x}_{k|k-1}$ (the predicted target state) and covariance $P_{k|k-1}$. Denote the probability of the $z_i[k]$ being the correct measurement at time index k as $\beta_i[k]$, whose expression will be described later. Now each validated

measurement is associated with a probability as its weight. Supposing that there are m_k validated measurements, the state estimator equation is described by

$$\hat{x}[k|k] = \hat{x}[k|k-1] + F[k]\nu[k] \tag{3.12}$$

where

$$\nu[k] = \sum_{i=1}^{m_k} \nu_i[k]\beta_i[k] \tag{3.13}$$

is the innovation variable;

$$\nu_i[k] = z_i[k] - \hat{z}[k|k-1] \tag{3.14}$$

is the distance from the real measurement to the predicted point;

$$F[k] = P[k|k-1]H_s^T S^{-1}[k] \tag{3.15}$$

is the feedback gain; and

$$S[k] = H_s P[k|k-1]H_s^T + V[k] \tag{3.16}$$

is the innovation covariance.

In the last equation, $V[k]$ is the measurement noise covariance at time index k, which can be calculated by:

$$V[k] \approx \frac{\sigma_r^2 - r^2\sigma_\alpha^2}{2} \begin{bmatrix} b + cos(2\alpha) & sin(2\alpha) \\ sin(2\alpha) & b - cos(2\alpha) \end{bmatrix}, \tag{3.17}$$

where

$$b = \frac{\sigma_r^2 + r^2\sigma_\alpha^2}{\sigma_r^2 - r^2\sigma_\alpha^2}, \tag{3.18}$$

r and α are the polar coordinates converted from the predicted target position at time index k, and σ_r and σ_α are the standard deviations of the associated measurement noise.

It is clear from the above equations that all the validated measurements are combined according to their probability of being the correct measurements and the weighted sum is used to update the estimation mechanism. Because the way the probabilities are assigned, those measurements that are closer to the predicted point receive higher weights because they are more likely to be the correct measurements.

Now the validation condition is introduced. All the validated measurements have to satisfy:

$$\nu_i{}^T[k]S^{-1}[k]\nu_i[k] \leq \gamma. \tag{3.19}$$

The above condition is used to determine a neighborhood around the predicted point, since $\nu_i[k]$ is the deviation of the ith measurement from the predicted point at time index k. Since the LIDAR measurements are two-dimensional (in the horizontal plane), the bound γ is determined from χ-squared tables with 2 degrees of freedom corresponding to the probability α_1 of rejecting the correct LIDAR measurements. Only the measurements which fall into this neighborhood are used to update the estimation. It is clear that the validation region increases with both γ and the innovation covariance $S[k]$. When uncertainty increases in the measurements, i.e. $S[k]$ becomes larger, the validation region increases to include

more candidate measurements.

The estimation error covariance is

$$P[k|k] = \beta_0[k]P[k|k-1] + (1-\beta_0[k](I - F[k]H_s) \\ P[k|k-1]F[k][(\sum_{i=1}^{m_k} v_i[k]v_i^T[k]\beta_i[k]) - v[k]v^T[k]]F^T[k] \tag{3.20}$$

The probability weighting $\beta_i[k]$ are computed by using Bayes' Rule.

$$\beta_0[k] = \frac{(\frac{m_k(\alpha_1+\alpha_2-\alpha_1\alpha_2)}{\Omega[k](1-\alpha_1)(1-\alpha_2)})}{\frac{m_k(\alpha_1+\alpha_2-\alpha_1\alpha_2)}{\Omega[k](1-\alpha_1)(1-\alpha_2)} + \sum_{j=1}^{m_k} p(z_j[k]|\chi_j[k], Z^{k-1}, m_k)} \tag{3.21}$$

$$\beta_i[k] = \frac{p(z_i[k]|\chi_i[k], Z^{k-1}, m_k)}{\frac{m_k(\alpha_1+\alpha_2-\alpha_1\alpha_2)}{\Omega[k](1-\alpha_1)(1-\alpha_2)} + \sum_{j=1}^{m_k} p(z_j[k]|\chi_j[k], Z^{k-1}, m_k)} \tag{3.22}$$

for $i = 1, ..., m_k$. where

$$p(z_i[k]|\chi_i[k], Z^{k-1}, m_k) = \frac{e^{-\frac{1}{2}\nu_j^T[k]S^{-1}[k]\nu_j[k]}}{2(1-\alpha_1)\pi\sqrt{|S[k]|}} \tag{3.23}$$

is a conditional probability density function;

$$\Omega[k] = \pi\gamma|S[k]|^{\frac{1}{2}} \tag{3.24}$$

is the area of the validation region (an ellipse for the two-dimensional case);

$$Z[k] = \{z_i[k]\}_{i=1,...,m_k} \tag{3.25}$$

is the set of all validated measurements at time index k;

$$Z^k = \{Z[j]\}_{j=1,...,k} \tag{3.26}$$

is the set containing all previous validated measurements up to time index k;

$$\chi_i[k] = \{z_i[k] \textit{ is the correct measurement}\}, i = 1, ..., m_k; \tag{3.27}$$

$$\chi_0[k] = \{none\ of\ the\ validated\ measurements\ is\ correct\}; \tag{3.28}$$

and α_2 is the probability for the case that the correct position is not detected by the LIDAR sensor.

The intensity data is not used in the above probability weightings. To incorporate it, let the intensity of the measurement $z_i[k]$ be denoted by $I_i[k]$. The probability weightings should then be changed to:

$$\beta_0[k] = \frac{\left(\frac{m_k(\alpha_1+\alpha_2-\alpha_1\alpha_2)I_0[k]}{\Omega[k](1-\alpha_1)(1-\alpha_2)}\right)}{\frac{m_k(\alpha_1+\alpha_2-\alpha_1\alpha_2)I_0[k]}{\Omega[k](1-\alpha_1)(1-\alpha_2)} + \sum_{j=1}^{m_k} p(z_j[k]|\chi_j[k], Z^{k-1}, m_k)I_j[k]} \tag{3.29}$$

$$\beta_i[k] = \frac{p(z_i[k]|\chi_i[k], Z^{k-1}, m_k)I_i[k]}{\frac{m_k(\alpha_1+\alpha_2-\alpha_1\alpha_2)I_0[k]}{\Omega[k](1-\alpha_1)(1-\alpha_2)} + \sum_{j=1}^{m_k} p(z_j[k]|\chi_j[k], Z^{k-1}, m_k)I_j[k]} \tag{3.30}$$

for $i = 1, ..., m_k$.

Chapter 4

LIDAR Based Autonomous Vehicle Following

4.1 Introduction

Compared to road following control, vehicle following control schemes have received much less attention in past research. This makes autonomous vehicle following a relatively new approach for vehicle steering control. Autonomous vehicle following achieves vehicle lane-keeping performance by controlling the vehicle to follow the preceding vehicle, assuming that the preceding vehicle is on the desired track with no lateral error nor relative yaw error with respect to the road centerline. In this control scheme, the lateral controller sets the steering command according to the vehicle's relative position with respect to the preceding vehicle.

Hence, no road infrastructure is required for the implementation of the control scheme. Autonomous vehicle following may serve as a back-up system for the road following based vehicle lateral control schemes in the case of sensor failures, and it may also work as an independent drive-assist system. In order to control the vehicle to follow the preceding vehicle, autonomous following schemes require the measurements of the relative distance between the two vehicles. This is achieved by the on-board laser scanning radar sensor (LIDAR) in this dissertation.

Algorithms have been developed in past for autonomous vehicle following. Fujioka and Omae described five vehicle following control algorithms by using a laser scanning radar(10), and Gehrig and Stein developed a trajectory-based algorithm for car following(11). These algorithms have to depend on a combination of many on-board sensors such as yaw rate sensor, accelerator, and sensors that detect the vehicle's relative position with respect to its preceding vehicle. Since no road reference system was available in their research, the lane-keeping performance for autonomous vehicle following has not been studied.

In practice, the preceding vehicle is not necessarily on the desired track. The lateral error and yaw of the preceding vehicle will be passed on to the following vehicle, when the following vehicle follows the path of the preceding vehicle. Since it is impossible for the controlled vehicle to follow the preceding vehicle perfectly, the controlled vehicle will have larger lateral errors than the preceding vehicle. If there are many vehicles under autonomous vehicle following control in a platoon,

and each of them follows its preceding vehicle except the leading one, the lateral errors of the following vehicles may be accumulated. Thus the string stability problem of the platoon must be studied in the lateral direction.

This chapter first describes the design of controllers for LIDAR-based autonomous vehicle following, including a lead-lag controller and a H_∞ controller. By analyzing the experimental results for the two control laws, with different control algorithms for the leading vehicle, the chapter tries to reveal the error propagation problem in practice. The error propagation/string stability problem is further studied by simulations and analysis. An inter-vehicle communication based solution is proposed, and the lane-keeping performance of the system is evaluated by real-time experiments involving two vehicles. Finally, simulations are conducted to verify the system performance for a platoon of four vehicles.

4.2 Design Issues

The main difference between vehicle following and road following is due to the coordinate frames where the sensor measurements are obtained from. In road-following control, on-board sensors, either magnetometers or vision sensors, measure the position of the vehicle with respect to an absolute coordinate frame (e.g. road reference frame), while in vehicle-following control, the sensors such as LIDAR can only measure the ego-vehicle's position relative to another moving vehicle. Thus the fundamental issue in designing a vehicle-following control system

is to decide the desired trajectory of the ego-vehicle. Once the desired trajectory of the ego-vehicle is determined, there is not much difference between the design for vehicle-following and that of road-following controllers because the vehicle dynamics are the same, despite the data manipulation of different types of sensors.

In terms of how to generate the desired trajectory, several schemes have been proposed by previous researchers. The ego-vehicle may go through a straight line towards the lead vehicle, or negotiate a curve which is predefined by the computer to reach the lead vehicle, or follow the trajectory of the lead vehicle point by point by storing the relative position data from the on-board sensors. In this chapter, the ego-vehicle is controlled to follow directly the lead vehicle according to the information from LIDAR. The input signal into the controller is the relative lateral distance between these two vehicles, and the LIDAR is considered as simply a sensor which provides certain look-ahead distance.

A reasonable question concerning this type of controller design is how L, the longitudinal distance between the two vehicles, affects the system performance. As shown in Fig.4.1, while the controller uses the deviation error of the following vehicle at L distance ahead as the feedback, the ego-vehicle tends to cut the curve, and the system error of using this method can be calculated quantitatively. In this figure, L is the distance between the two vehicles, R is the road radius, and α is the angle as shown. It is known that the road curvature of highways cannot be

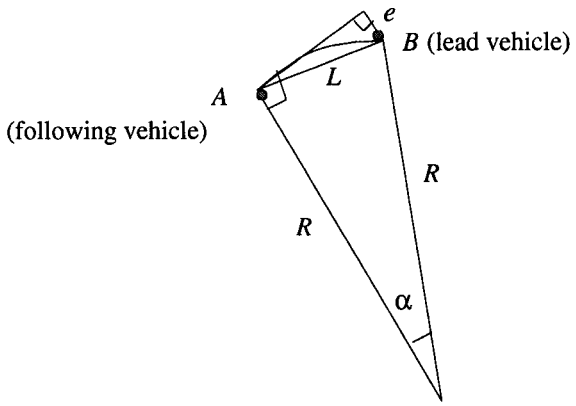

Figure 4.1: System error of the control scheme

larger than 0.00125 $[1/m]$; then the worst-case system error is:

$$e = \frac{L^2}{2R} \tag{4.1}$$

Since most current magnetometer-based lateral controllers use a virtual look-ahead scheme as described in Chapter 2, i.e. the controllers compute the lateral deviation at a distance ahead of vehicle CG, the worst-case system error for the vehicle following scheme compared to the look-ahead scheme is only

$$e_r = \frac{L^2 - h^2}{2R} \tag{4.2}$$

where h is the look-ahead distance used by current magnetometer-based lateral controllers.

Assuming h as 4 m, which is a reasonable virtual look-ahead distance, the worst-case system error (when R is 800 m) is 5 cm for $L = 10$ m. Thus for small following distance, this control scheme is acceptable. The Bode plots of the open

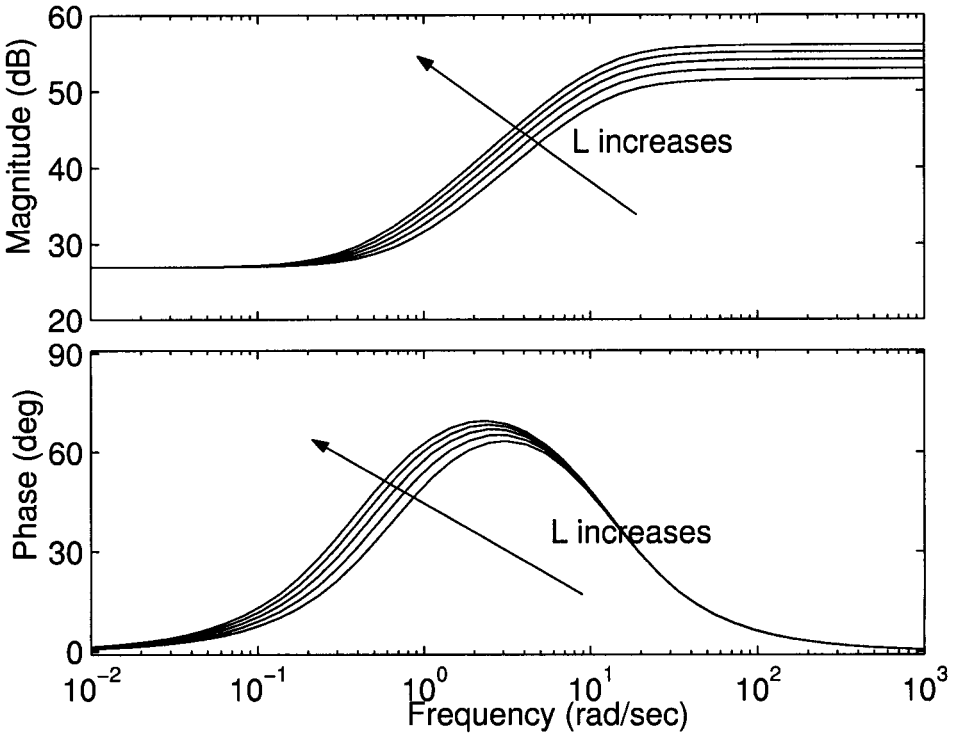

Figure 4.2: Effects of look-ahead distance on the open loop system dynamics (for vehicle velocity $= 8m/s$, and $L = 8, 10, 12, 14, 16m$)

loop transfer function from the steering input to the lateral acceleration of the vehicle are shown in Fig.4.2.

4.3 Setup for Experimental Study

A platoon of two Buick vehicles were used in the experimental testing on a test track at the Richmond Field Station, University of California, Berkeley. The maximum allowable speed on the test track was 25MPH. The track consisted of many curves, but no preview of the road curvature was used in the testing. The unique feature of this track was that there were equally-spaced magnetic markers

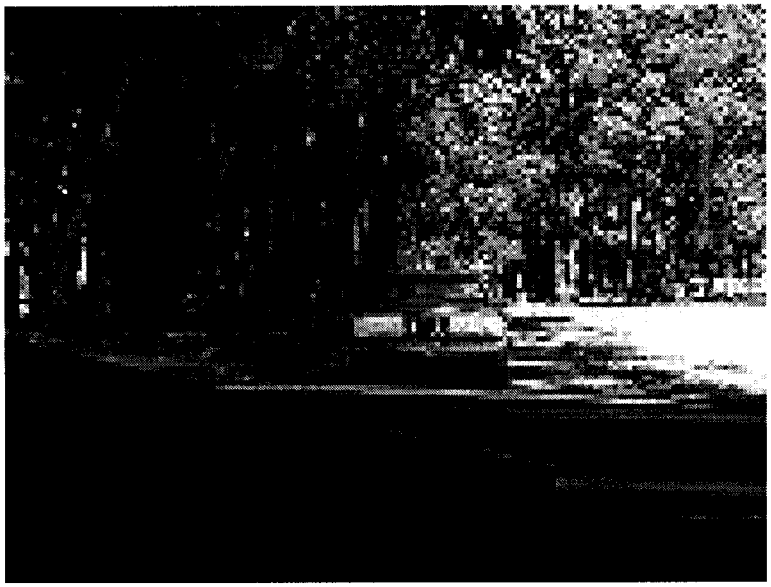

Figure 4.3: Autonomous vehicle following experiment (the vehicle in the center of the picture is the lead vehicle; the vehicle at the bottom of the picture, which is not shown completely, is the following vehicle)

buried under the road centerline. Both test vehicles were equipped with two sets of magnetometers, one under the front bumper and the other under the rear bumper. Hence the magnetometer measurements represent the vehicles' lateral deviation from the road centerline. The two vehicles were manually driven in the longitudinal direction, and the space between them was controlled manually by the driver who operated the following vehicle. In the testing, the leading vehicle was automatically steered based on the magnetometer measurements to follow the magnetic markers, i.e. the road centerline, and the following vehicle used the autonomous vehicle following based steering control. The magnetometer measurements on the following vehicle were never used to set the steering control input, but they were collected to evaluate the vehicle's tracking performance in the road-fixed coor-

dinate frame. Comparison between the magnetometer measurements of the two vehicles will further reveal the potential error propagation problem in autonomous vehicle following.

4.4 Lead-Lag Control

The controller design starts with the assumption that there is no communication between the leading and the following vehicles. Thus the dynamics of the leading vehicle are treated as unknown disturbances to the following vehicle. The input to the controller is the relative lateral distance measured by the LIDAR sensor, and the design of the autonomous vehicle following controller is similar to that for a road following controller, except that the vehicle dynamic system has a large and fixed look-ahead distance. The first control algorithm used here is a lead-lag controller. The control law is:

$$\frac{(2s+1)(18s+1)}{(0.2s+1)(56.98s+1)} \tag{4.3}$$

The Bode plot of this controller is shown in Fig.4.4.

Figures 4.5 and 4.6 show the experimental results of the controlled vehicle. The vehicle following performance is evaluated by the measurements from both the LIDAR and the magnetometer sensors. It can be seen from the results that the controlled vehicle is still kept in the lane by following the lead vehicle. However, there is a negative bias associated with the lateral position of the following vehicle,

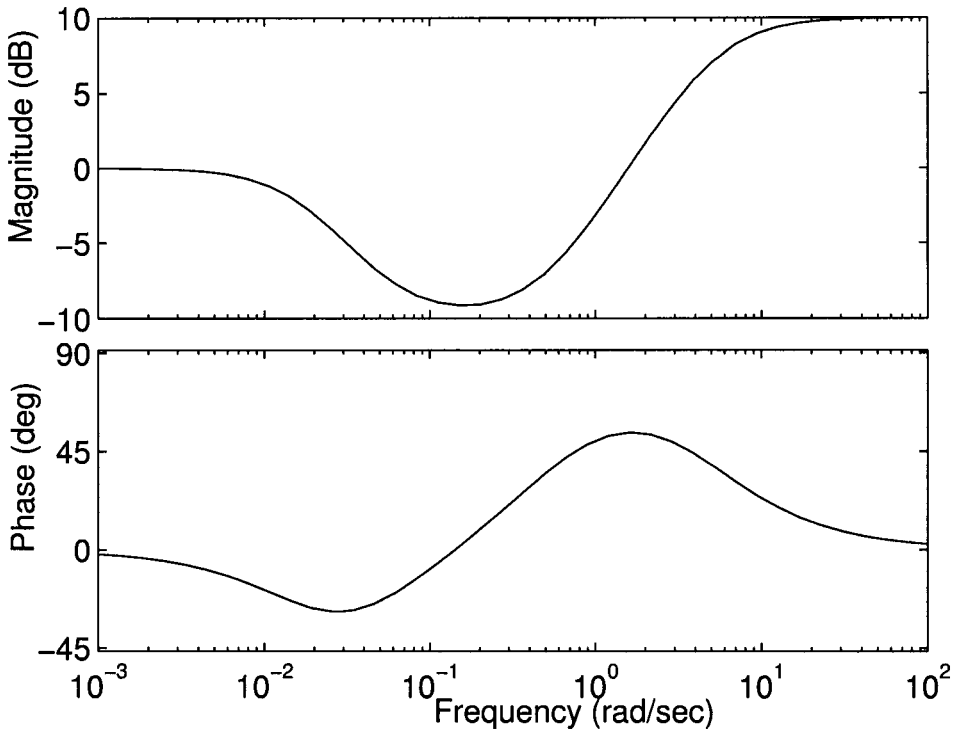

Figure 4.4: Bode plot of the autonomous vehicle following controller

relative to the road centerline. The control law of the leading vehicle was one of the existing steering controllers. Due to technical difficulties, the sensor measurements of the two vehicles when the leading vehicle was using this control law could not be synchronized. Hence the experimental results of the leading vehicle are shown separately in Fig.4.7. Note that there is also a small negative bias in the lateral deviation of the leading vehicle. By comparing the lane-keeping performance of the two vehicles, one may conclude immediately that the performance of the following vehicle is worse than that of the leading one; further, one may guess that the large bias for the following vehicle may be caused by the small bias of the leading vehicle. Intuitively, this is a reasonable hypothesis because any lateral error of the leading vehicle may be transmitted to the vehicle that follows its trajectory. In general, the tracking error should become worse in the following vehicle.

4.5 H_∞ Synthesis

The second controller is designed by using H_∞ synthesis. In this design, the control algorithm is required to calculate the correct steering angle at the tires in order to regulate the lateral deviation, in the presence of the unknown road curvature and sensor noise. The steering input should be kept small considering the saturation problems and passenger discomfort. As shown in Fig.4.8, G is used to represent the vehicle lateral dynamics described in Chapter 2, the road curvature is treated as an unknown disturbance d, n denotes the sensor noise, and

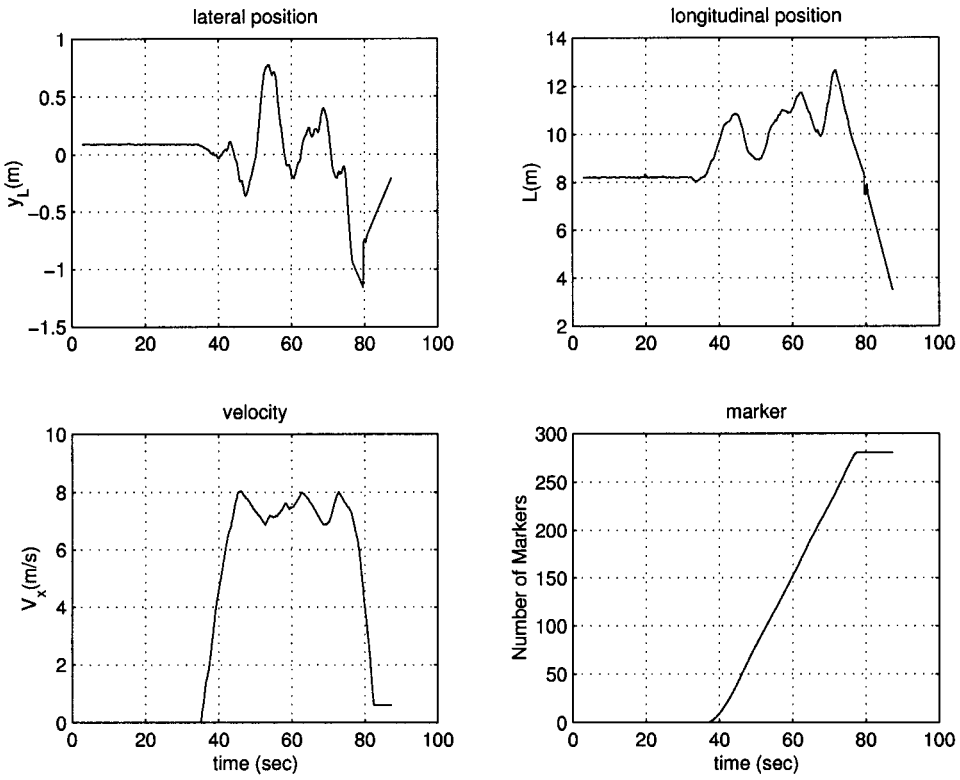

Figure 4.5: Lead-lag control experimental results of following vehicle when the tracking error of the leading vehicle has a negative bias: lateral and longitudinal distance measured by LIDAR sensor, vehicle velocity, and recording of magnetic markers

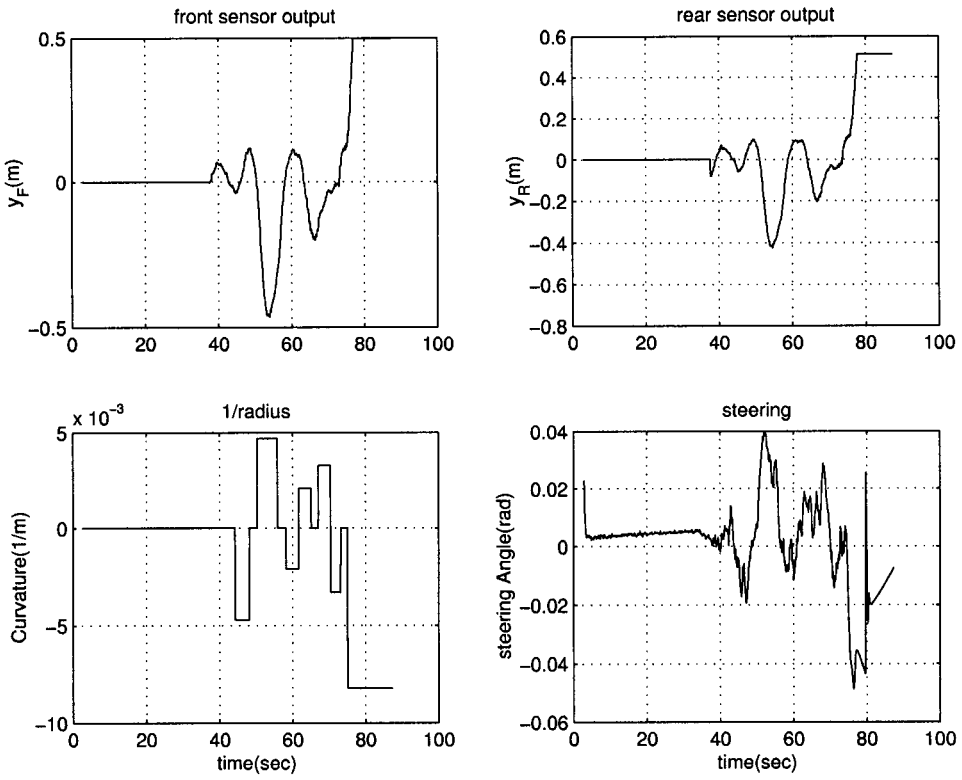

Figure 4.6: Lead-lag control experimental results of following vehicle when the tracking error of the leading vehicle has a negative bias: measurements from front and rear magnetometers, road curvature, and steering angle

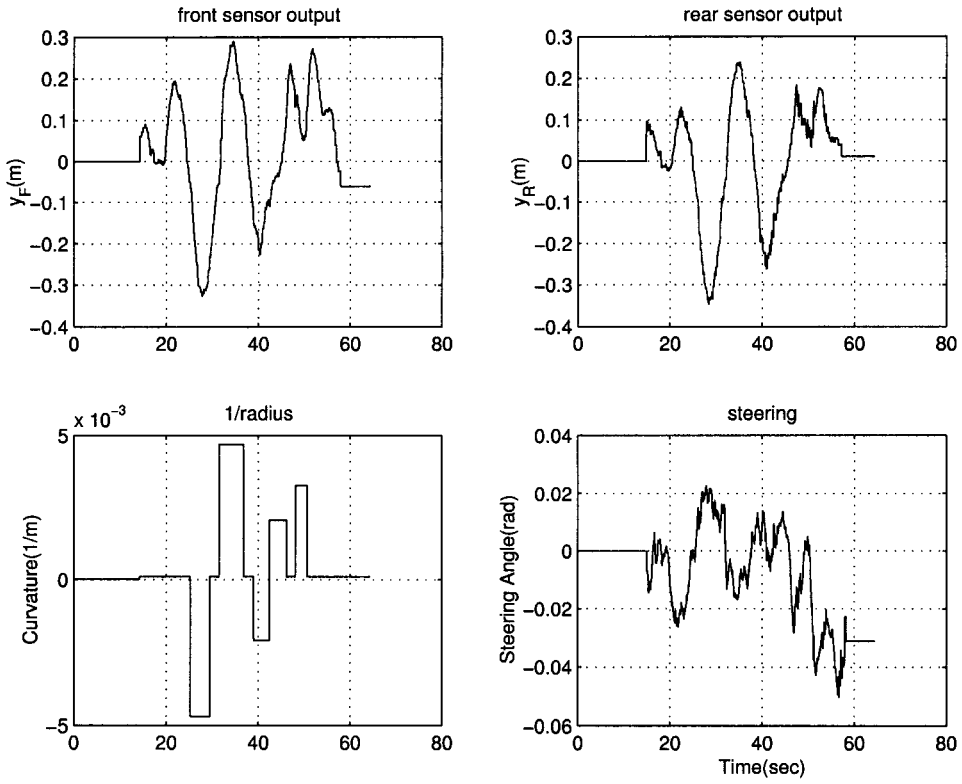

Figure 4.7: Experimental results of lead vehicle associated with a negative bias: measurements from front and rear magnetometers, road curvature, and steering angle

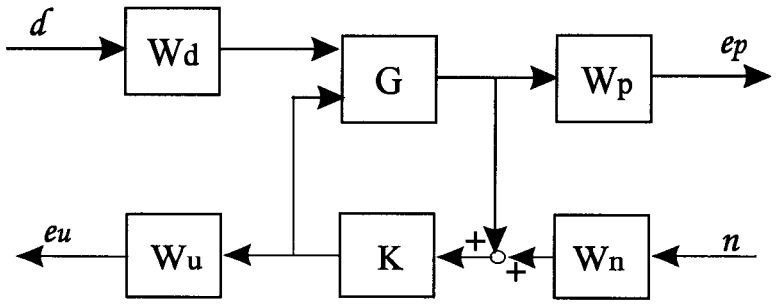

Figure 4.8: H_∞ synthesis structure

the weighting functions W_p, W_n, W_u, and W_d are used to place suitable weights at various frequency ranges. e_p and e_u are the weighted vehicle lateral deviation and steering input, respectively. The goal of this design is to minimize the effects of the external disturbances d and n on the weighted system outputs in terms of the H_∞ norm.

The weighting functions are chosen according to standard considerations in H_∞ synthesis design. Penalty on the lateral error should be high at low frequencies for good tracking performance, and low at high frequencies to avoid exciting the unmodeled high-frequency dynamics. For the same reason, penalty on the steering input should be high at high frequencies. W_n and W_d are set constant to avoid producing a high-order controller, and they are chosen according to the system performance requirements. The weighting functions chosen for this design are as follows.

$$W_d = \frac{7}{200} \tag{4.4}$$

$$W_n = \frac{1}{50} \tag{4.5}$$

$$W_p = 0.1\frac{s+1}{s+0.003} \tag{4.6}$$

$$W_u = 2000\frac{s+10}{s+120} \tag{4.7}$$

The controller thus designed is of sixth-order.

The control algorithm for the leading vehicle was redesigned in a lead-lag form, and this also enabled the synchronization of the recording of the two vehicles' performance. Figures 4.9 and 4.10 show the experimental results of the autonomous

vehicle following control while the redesigned controller for the lead vehicle and the H_∞ controller for the following vehicle were used. Both vehicles traveled up to 20MPH during the testing. Note that the steering controller of the leading vehicle was different from that in the previous testing. The maximum tracking error of the lead vehicle was about $10cm$ from the road centerline, and the maximum tracking error of the following vehicle was about $25cm$ from the road centerline. Therefore the tracking performance of this controller is significantly better than the previous one. From the results, it is clear that the lateral deviation of the following vehicle now has a large positive bias. It is also computed that the average of the lateral deviation of the lead vehicle was about positive $5cm$, and this could be the reason for the positive bias in the tracking error of the following vehicle. Again the results have verified the previous hypothesis that the lateral error of the lead vehicle indeed has been transmitted to the following vehicle. It is clear that without additional information, autonomous following algorithm can not adjust the bias in real time.

4.6 String Stability in Autonomous Following

The above experimental results have shown that tracking errors of the leading vehicle may be passed on to the following vehicle and result in larger errors of the following vehicle. One may still wonder whether this is true for a larger platoon of vehicles. This problem is illustrated by simulation results for a platoon of four

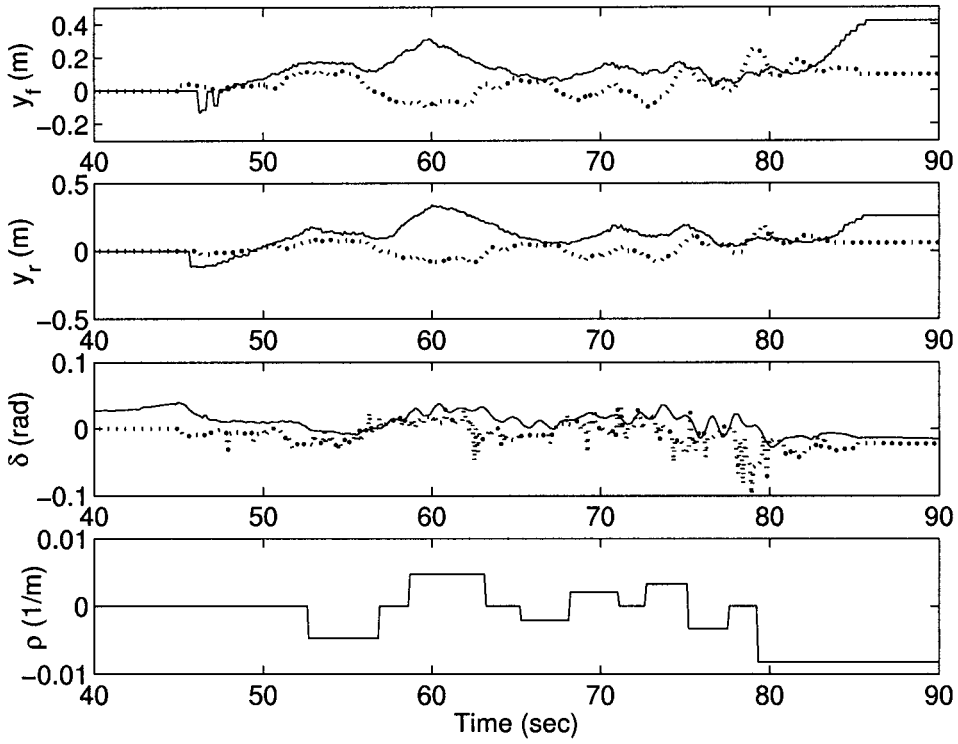

Figure 4.9: H_∞ control experimental results for autonomous vehicle following when the tracking error of the leading vehicle has a positive bias: front, rear magnetometer outputs, steering angle, and road curvature. (solid: following vehicle; dashed: lead vehicle)

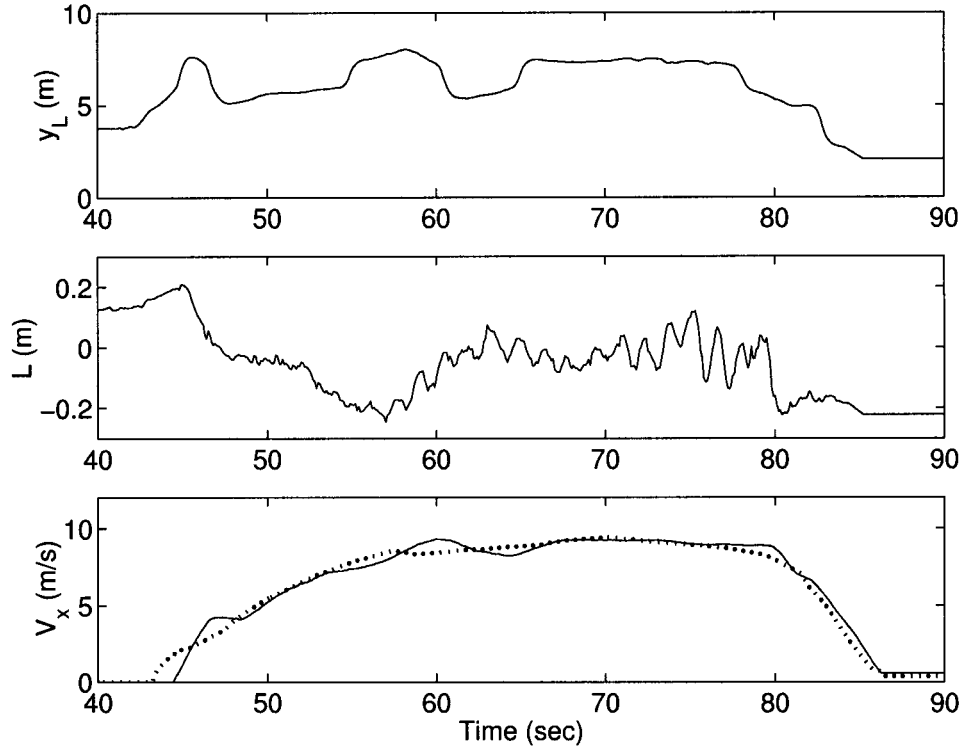

Figure 4.10: H_∞ control experimental results for autonomous vehicle following when the tracking error of the leading vehicle has a positive bias: lateral, longitudinal distance between the two test vehicles measured by LIDAR, and vehicle speed (solid: following vehicle; dashed: lead vehicle)

vehicles. In the simulation, the first vehicle of the platoon used a road-following control algorithm, and the other vehicles were under autonomous vehicle following control, each one following its preceding vehicle. The simulated road consisted of two curves, each with curvature of $\pm\frac{1}{800m}$ respectively, as shown in Fig.4.11. The simulated vehicle speed was $30m/sec$ for all vehicles. The space between adjacent vehicles was $10m$. The simulation results are shown in Fig.4.12. It can be seen that the lateral deviation accumulates in the upstream direction of the platoon, i.e. the lateral error of each following vehicle is larger than that of its preceding vehicle. The accumulation of tracking errors is caused by the superposition of the tracking errors of the leading vehicle and the errors in autonomous vehicle following. As the number of the following vehicles increases, the tracking errors of the vehicle at the end of the platoon increase. Note that the control system of each vehicle in the simulation is stable, but the simulation results still indicate the stability issue for vehicle platoons, i.e. string stability.

In order to analyze the string stability problem in autonomous vehicle following, the following definitions and theorem from Swaroop and Hedrick (30) are introduced.

Consider the following interconnected system:

$$\dot{x}_i = f(x_i, x_{i-1}, \cdots, x_{i-r+1}) \tag{4.8}$$

where $i \in N$, $x_{i-j} \equiv 0$, $\forall i \leq j$, $x \in R^n$,

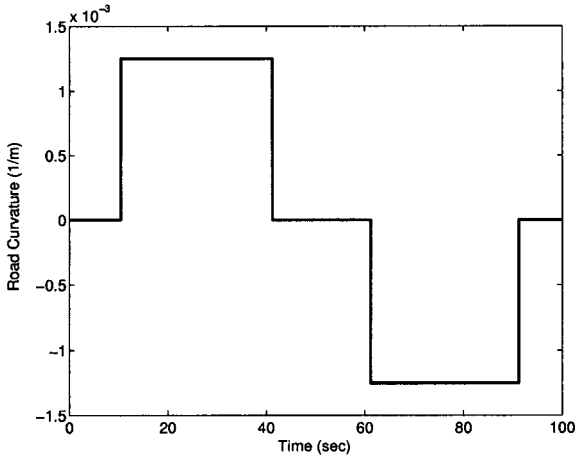

Figure 4.11: Simulated road curvature)

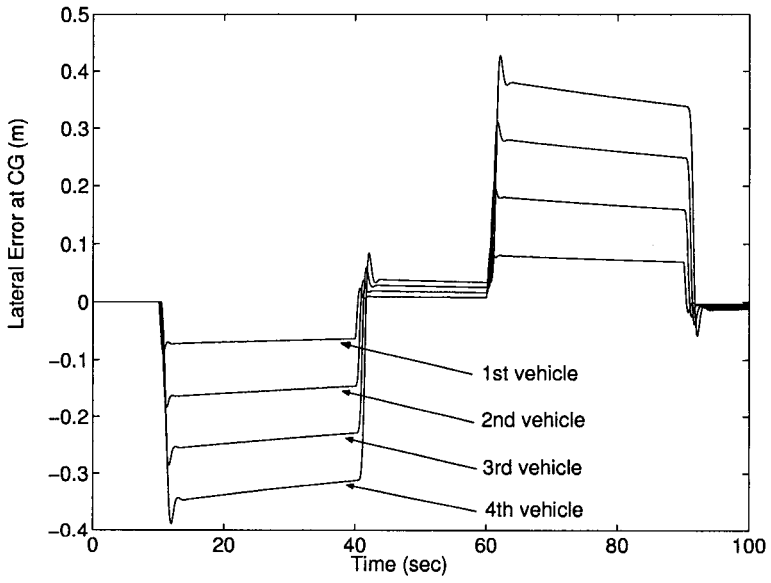

Figure 4.12: Simulation results for autonomous vehicle following control without inter-vehicle communication (for a platoon of four vehicles)

$$f: \underbrace{R^n \times \cdots \times R^n}_{r \text{ times}} \rightarrow R^n \quad \text{and } f(0, \cdots, 0) = 0.$$

Definition 1: The origin $x_i = 0$, $i \in N$ of (4.8) is string stable, if given any $\epsilon > 0$, there exists a $\delta > 0$ such that $||x_i(0)||_\infty < \delta \Rightarrow sup_i ||x_i(\cdot)||_\infty < \epsilon$.

Definition 2: The origin of the interconnected system $x_i = 0$, $i \in N$ of (4.8) is asymptotically (exponentially) string stable if it is string stable and $x_i(t) \rightarrow 0$ asymptotically (exponentially) for all $i \in N$.

Theorem (Weak Coupling Theorem for String Stability)(30): If the following conditions are satisfied:

- f is globally Lipschitz in its arguments, i.e.,

$$\begin{aligned} &|f(y_1, \cdots, y_r) - f(z_1, \cdots, z_r)| \\ \leq &l_1|y_1 - z_1| + \cdots + l_r|y_r - z_r|. \end{aligned} \tag{4.9}$$

- The origin of $\dot{x} = f(x, 0, \cdots, 0)$ is globally exponentially stable.

Then for sufficiently small l_i, $i = 2, \cdots, r$, the interconnected system is globally exponentially string stable.

The above theorem provides a sufficient condition for string stability of an interconnected system, and it shows that string stability can be achieved if the coupling between the system components is sufficiently weak.

For the steering control of the ith vehicle in autonomous vehicle following, the feedback signal is the vehicle's lateral distance from the preceding vehicle. Hence, by neglecting the road curvature,

$$\dot{x_i} = Ax_i + B\delta_i \tag{4.10}$$

$$\delta_i = -Ky_{Li} \tag{4.11}$$

where K is the steering control gain. According to Eqn.(2.27),

$$\begin{aligned} \delta_i &= -K(y_{Vi} - y_{Ri-1}) \\ &= -K(C_2x_i - C_1x_{i-1}) \end{aligned} \tag{4.12}$$

Then,

$$\begin{aligned} \dot{x_i} &= Ax_i + B(-K(C_2x_i - C_1x_{i-1})) \\ &= (A - BKC_2)x_i + BKC_1x_{i-1} \\ &= g(x_i, x_{i-1}) \end{aligned} \tag{4.13}$$

It is clear from the above equations that the feedback control system of the ith vehicle is coupled with that of the $(i-1)$th vehicle, and hence the vehicle platoon forms an interconnected system. It can be shown that

$$\begin{aligned} &|g(y_1, y_2) - g(z_1, z_2)| \\ \leq &|A - BKC_2| \cdot |y_1 - z_1| + |BKC_1| \cdot |y_2 - z_2| \end{aligned} \tag{4.14}$$

The above expression shows that to make the coupling weak, the magnitude of the controller K has to be sufficiently small. Clearly, this is not a practical solution.

4.7 Inter-Vehicle Communication Based Approach

According to Eqn.(2.27), if the absolute position of the rear end of the $(i-1)$th vehicle y_{Ri-1} is known, the coupling between the ith and the $(i-1)$th vehicle vanishes. Measurements of y_{Ri-1} may become available to the $(i-1)$th vehicle, if the vehicle is equipped with appropriate sensors such as GPS, vision camera, or magnetometers. Then through inter-vehicle communication, measurements of a leading vehicle, e.g.the $(i-1)$th vehicle, are shared by all the following vehicles. The vehicle directly following the leading vehicle may compute

$$y_{Vi} \approx (y_{Li} - y_{Ri-1}) \tag{4.15}$$

Note that y_{Vi} is the lateral deviation, at a point with distance L ahead of vehicle CG, relative to the road centerline, and it does not depend on the preceding vehicle. Now the following vehicle may use y_{Vi} as the feedback signal to the control algorithm. Then, the tracking performance of the vehicle should not depend on that of the preceding vehicle.

Inter-vehicle communication between the vehicles was achieved through Utilicom radios. At constant time steps (every $20msec$), the lead vehicle sent its measurements of the rear magnetometers (under rear bumper) to the following vehicle. The lead vehicle was under automated steering control with the magnetometer measurements as the feedback signal, but the following vehicle used only LIDAR measurements and communicated information from the lead vehicle. The same H_∞ controller as described previously was used for the following vehicle. Again,

due to technical difficulty, the leading vehicle only used the redesigned controller, which is in lead-lag form and generates a positive bias in tracking errors as shown in Figs.4.9 and 4.10, because synchronization was required in order to enable the communication process.

The experimental results of the autonomous vehicle following control with inter-vehicle communication are shown in Fig.4.13 and Fig.4.14. The results show that with inter-communication not only was the lateral deviation of the following vehicle significantly reduced, but also the bias disappeared. Note that the speed of the test vehicles was up to 25MPH, a little higher than that in the previous tests. The reason for performance improvement is that the control algorithm regulated the vehicle's absolute deviation, at the point L ahead of vehicle CG, from the road centerline, instead of the relative deviation from the lead vehicle. This was achieved by using inter-vehicle communication and combining LIDAR measurements with the communicated information.

4.8 Simulation for a Vehicle Platoon

Simulations have been conducted to study the effects of inter-vehicle communication on vehicle performance and string stability for a larger vehicle platoon. Assuming that the 1st vehicle measures its absolute deviation y_{R_1} and communicates it to the following vehicles, the second vehicle calculates y_{V_2} by combining the communicated information with LIDAR measurements. However, since the

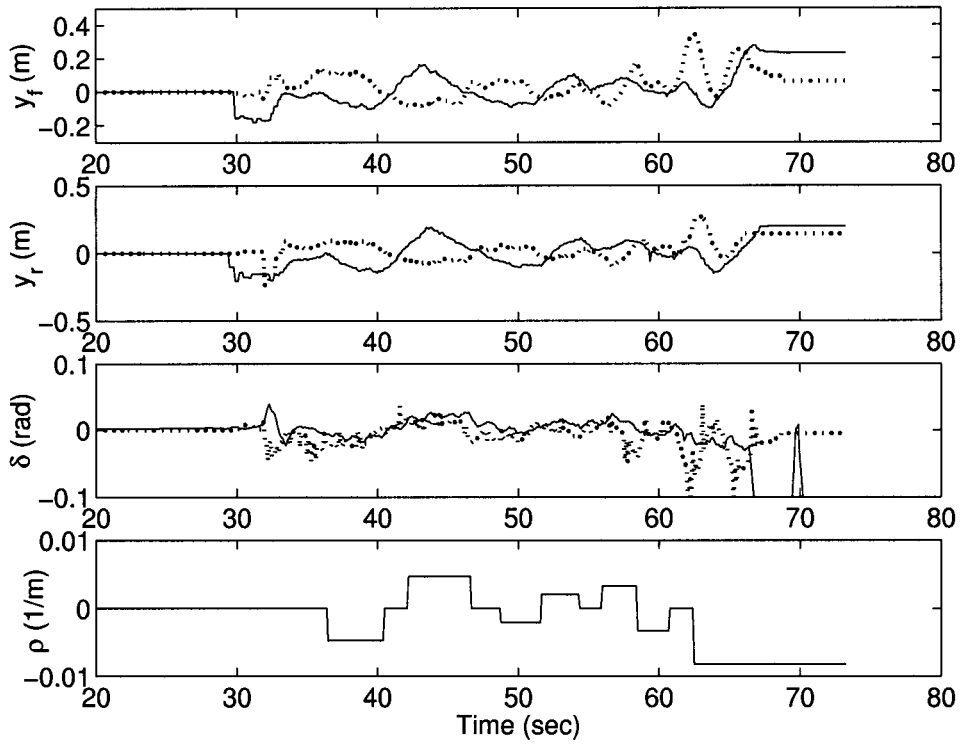

Figure 4.13: Experimental results for autonomous vehicle following with inter-vehicle communication: front, rear magnetometer outputs, steering angle, and road curvature. (solid: following vehicle; dashed: lead vehicle)

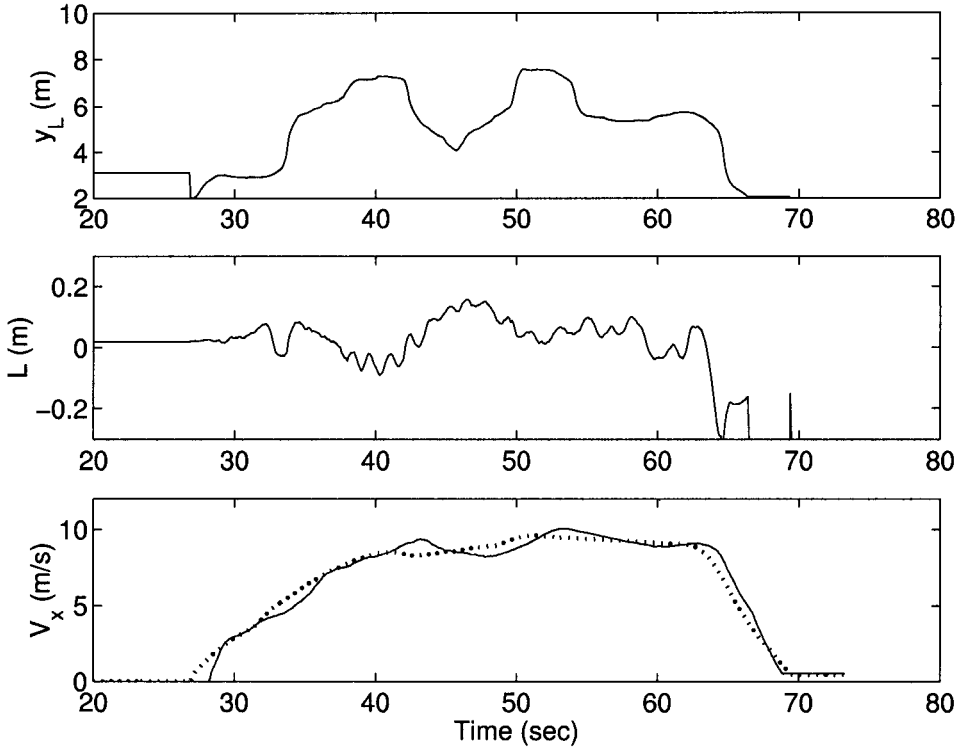

Figure 4.14: Experimental results for autonomous vehicle following with inter-vehicle communication: lateral, longitudinal distance between the two test vehicles measured by LIDAR, and vehicle speed (solid: following vehicle; dashed: lead vehicle)

second vehicle cannot measure y_{R2}, this algorithm stops and cannot be applied to the third vehicle. To solve the problem, a Kalman estimator is developed to estimate y_{R2} from y_{V2}. The problem is formulated for the ith vehicle as follows. For simplicity, the subscript i has been omitted.

$$\dot{x} = Ax + B\delta + Bw \tag{4.16}$$

$$y_V = C_2 x + v \tag{4.17}$$

where w is process noise, and v is measurement noise. The noise covariances are chosen as

$$E(ww') = 2.5e - 005; \tag{4.18}$$

$$E(vv') = 0.0004; \tag{4.19}$$

$$E(wv') = 0; \tag{4.20}$$

The estimator has input $[\delta; y_V]$, and it can compute the optimal estimate of the state variable $\hat{x}$. Clearly,

$$\hat{y_R} = C_1 \hat{x} \tag{4.21}$$

Then the estimated $\hat{y_R}$ can be communicated to the following vehicles, and the previous algorithm continues in the upstream direction of the platoon. The soundness of estimating y_{R2} by using y_{V2} is validated using the measurements from the previous experiments, as shown in Fig.4.15. The figure shows that most of the time the estimation error is about 5 to $8cm$.

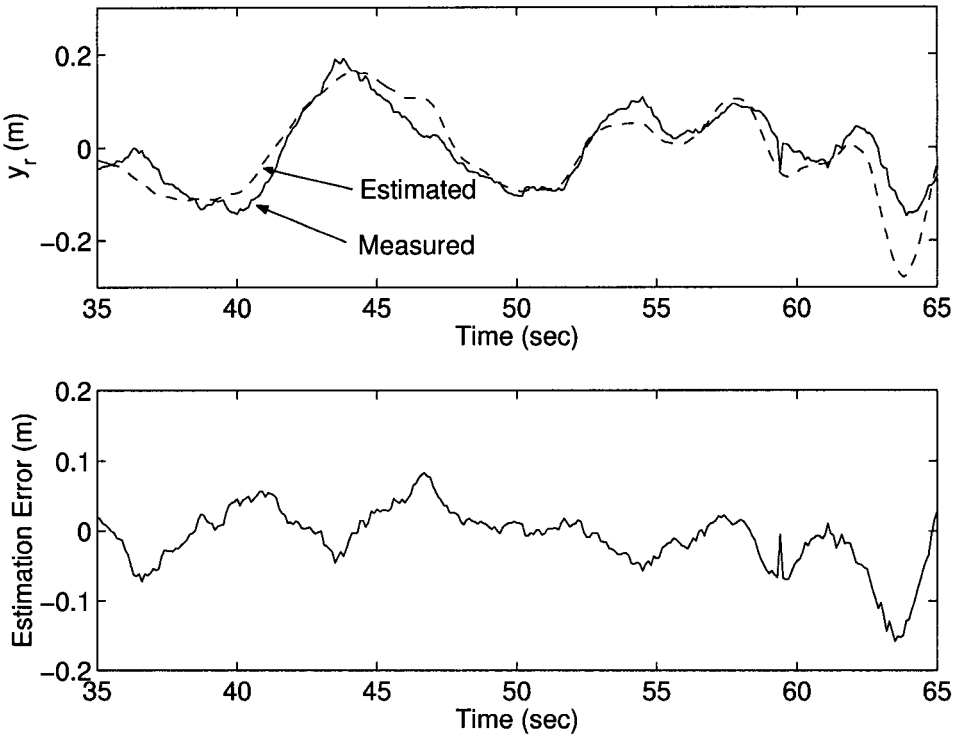

Figure 4.15: Estimation of y_R based on y_V and control input

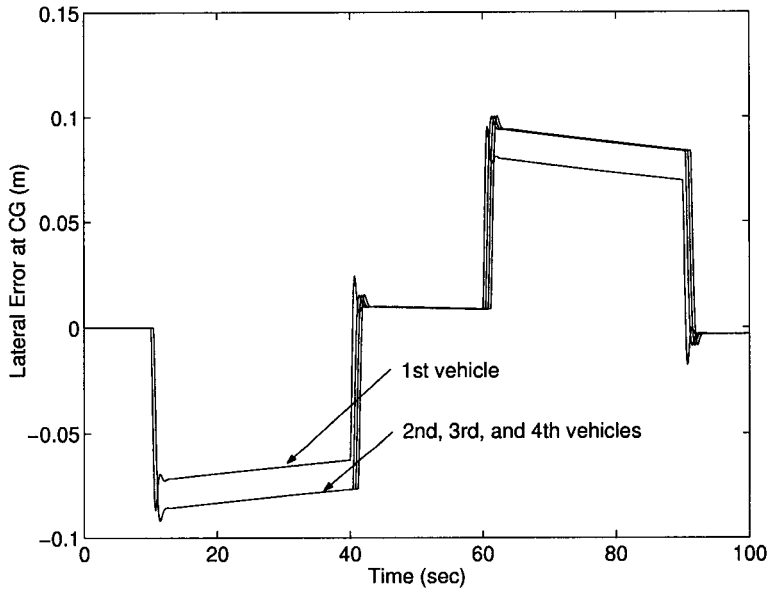

Figure 4.16: Simulation results for a platoon of four vehicles with perfect estimation

The simulation used a platoon of four vehicles, under the same condition as described in Section 4.6. In the first simulation, it was assumed that y_R is perfectly estimated, and the simulation results are plotted in Fig.4.16 as lateral deviation at the vehicle CG vs. time. The results show that with inter-vehicle communication, the lateral errors of the all the following three vehicles are almost the same, and the errors no longer accumulate in the upstream direction of the platoon.

Since the above results may seem optimistic to some extent, simulations have been conducted again with the assumption that each estimator generates $10cm$ random error. The results are plotted in Fig.4.17. It can be seen that even with the random noise in the simulation the tracking errors of the following vehicle do not accumulate as much as in Fig.4.12. These results show that inter-vehicle communication is a practical way to solve the string stability problem in

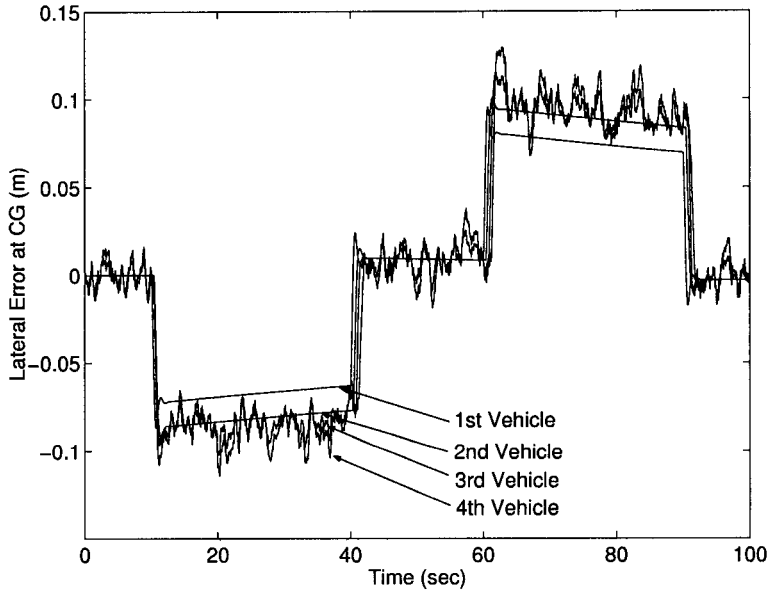

Figure 4.17: Simulation results for a platoon of four vehicles $10cm$ estimation error autonomous vehicle following.

4.9 Summary

This chapter presented a new scheme for autonomous vehicle following steering control of a passenger vehicle. Autonomous vehicle following allows a vehicle to automatically follow its preceding vehicle, based on real-time information of the relative distance between the two vehicles. In this work, the relative distance is measured by an on-board laser scanning radar sensor (LIDAR). Real-time testings were conducted on a test track which was equipped with a unique magnetic reference system. The error propagation problem in autonomous vehicle following was emphasized in this chapter, as it may eventually result in string instability of a

vehicle platoon. This problem was demonstrated repeatedly through two real-time testing results and a simulation result of a platoon of four vehicles. The string stability problem was analyzed for autonomous following, and the inter-vehicle communication approach was suggested as a solution. The controller uses measurements from both LIDAR and the communicated lateral deviation of the leading vehicle. Experimental results were presented to show that inter-vehicle communication effectively reduced the vehicle tracking errors in autonomous following. Simulation results were also presented to confirm that inter-vehicle communication helps solve the string stability problem for a larger platoon of vehicles.

Chapter 5

Integrated Steering Control

5.1 Introduction

In the previous chapter, it was shown that autonomous vehicle following may be used as an independent automatic steering control system. Hence it may work as a back-up system for road following control schemes during the total failure of road following sensors, e.g. magnetometers. Autonomous vehicle following may also become helpful to the road following schemes when the road following sensors partially fail. This chapter considers the sensor failure case for the magnetometer-based approach, but similar techniques should also be useful to other road following systems. The current magnetometer-based vehicle control schemes rely on two sets of on-board magnetometers, mounted under the front and rear bumpers. Failure in either set of the magnetometers leads to degraded steering performance, some-

times even causing instability. As shown in Chapter 2, front magnetometers are critical for vehicle lateral control. More precisely, if the front magnetometers fail, a right-half-plane zero appears on the pole-zero map of the input-output dynamics from the front wheel steering angle to the lateral error at the rear bumper, which may cause a substantial deterioration of the lane-keeping performance. However, the desired vehicle performance may be achieved by combining the rear magnetometers with the LIDAR sensor. Inclusion of the magnetometer measurements in vehicle following control may also reduce the dependence of the following vehicle on the lead vehicle. Under this integrated control scheme, the controlled plant, i.e. the vehicle, becomes a Single Input, Two Output (SITO) system: the front wheel steering angle is the input and the rear magnetometers and LIDAR define the two outputs. In the closed loop, disturbances associated with one system output may have strong effects on the other output. This may become a severe problem considering the strong disturbance associated with the LIDAR measurement, which is caused by the unknown dynamics of the leading vehicle. Freudenberg and Middleton(8) have p roposed the concepts of "direction" and "alignment" in analyzing general SITO systems. This chapter will first analyze the interactions of the SITO systems, and then propose a controller design procedure to achieve minimum interactions as well as stability and optimal performance under failure of front magnetometers.

5.2 Problem Formulation and Control Objectives

When the front magnetometers fail, the back-up system may utilize the rear magnetometers and the LIDAR sensor. It should be noted that the measurements of the LIDAR sensor are relative to the coordinate system fixed to the lead vehicle, while those of the rear magnetometers are relative to the road reference coordinate system. For the road reference system, LIDAR measurements can be considered as the composition of two parts, i.e. the position of the following vehicle at the LIDAR measurement location and the position of the rear of the preceding vehicle. The latter part depends on the dynamics of the preceding vehicle. It is assumed in this chapter that there is no communication between the vehicles, and the dynamics of the preceding vehicle are considered as unknown disturbances. Hence, the system outputs can be written as $y = H\xi$, where

$$H = \begin{bmatrix} 1 & 0 & L & 0 \\ 1 & 0 & -h_2 & 0 \end{bmatrix}, \tag{5.1}$$

and y is the measured system output. The physical meanings of L and h_2 can be found in Table 2.1. The first system output in the above equations is the measurement from the LIDAR sensor and the second one is from the rear magnetometers. Figure 5.1 shows the geometry of the sensor locations and measurements. Note that the output equation assumes that the LIDAR output of the following vehicle is equivalent to the lateral error measured by a (virtual) sensor located at L $[m]$ ahead of the following vehicle's CG. Disturbance d_1 is introduced to absorb the

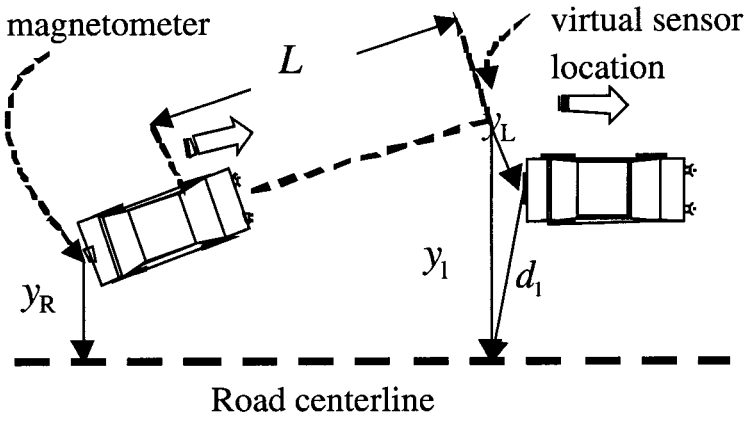

Figure 5.1: Geometry of sensor locations

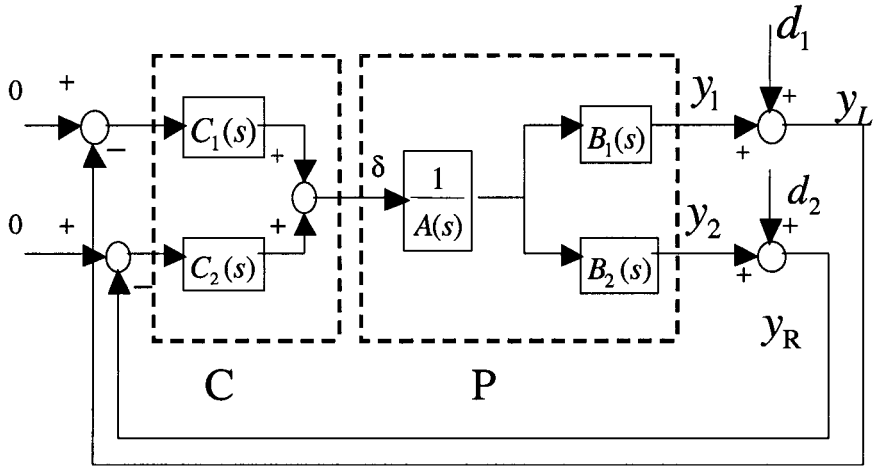

Figure 5.2: Control problem formulation

discrepancy between this assumption and the actual situation. The dynamics of the preceding vehicle may affect d_1.

The control system is shown in Fig.5.2, where P is the Single Input, Two Output (SITO) plant, y_L is the output of the LIDAR sensor, d_1 is the disturbance as described above, and d_2 is the disturbance associated with the measurements from the rear set of magnetometers, y_R. As described in Section 5.1, vehicle lateral control performance with the feedback signal from the rear magnetometer measurements alone is limited because of an unstable zero of the vehicle dynamics from δ to y_R. The benefit of using the information from the LIDAR sensor is that the dynamics from δ to y_L do not involve any unstable zeros. In fact, the zero appears in the left-half side of the s-plane. However, the disadvantage of using the LIDAR sensor is that the disturbance, due to the unknown actual position and dynamics of the preceding vehicle, may affect the performance in terms of following the road centerline. Measurements from the rear magnetometers may be helpful in order to bring the vehicle back to the road centerline because they provide accurate measurements of the lateral deviation of the vehicle. The optimal way of combining these two sensor outputs can be achieved by careful controller design, based on the integrated closed loop system analysis. The control objective is to design a Two Input Single Output (TISO) controller such that no significant interactions occur in this closed loop control system within the system bandwidth, i.e., disturbances associated with one channel should have minimum effects on the other channel

and vice versa. In particular, the effect of d_1 on the rear magnetometer loop should remain small. Moreover, the controller should internally stabilize the control system and achieve optimal closed loop system performance.

5.3 Properties of Single Input, Two Output Feedback Systems

In Fig.5.1, let

$$P(s) = \begin{bmatrix} p_1(s) \\ p_2(s) \end{bmatrix} = \begin{bmatrix} \frac{B_1(s)}{A(s)} \\ \frac{B_2 s}{A(s)} \end{bmatrix} \tag{5.2}$$

$$C(s) = \begin{bmatrix} c_1(s) & c_2(s) \end{bmatrix} \tag{5.3}$$

The output sensitivity function is

$$S_o(s) = \Big(I + P(s)C(s) \Big)^{-1} \tag{5.4}$$

Let

$$S_o(s) = \begin{bmatrix} S_{11} & S_{12} \\ S_{21} & S_{22} \end{bmatrix} \tag{5.5}$$

Then the system outputs are written as,

$$\begin{bmatrix} y_L(s) \\ y_R(s) \end{bmatrix} = S_o \begin{bmatrix} d_1(s) \\ d_2(s) \end{bmatrix} = \begin{bmatrix} S_{11}d_1 + S_{12}d_2 \\ S_{21}d_1 + S_{22}d_2 \end{bmatrix} \tag{5.6}$$

The above equation implies that d_1 affects y_R, and d_2 affects y_L, only through the off-diagonal terms of S_o. Therefore, it is important to minimize the magnitudes

of these terms. In particular, S_{21} should remain small. The following theorem is summarized from the work done by Freudenberg and Middleton(8).

Theorem: For a fixed open loop gain $L = CP$, $max(|S_{21}|, |S_{12}|)$ is lower bounded, and the lower bound can be achieved iff

$$\frac{c_2(j\omega)}{c_1(j\omega)} = conj(\frac{p_2(j\omega)}{p_1(j\omega)}) \tag{5.7}$$

where $conj(x)$ represents the complex conjugate of x.

Proof: Let T_I be the complementary sensitivity function, i.e.

$$T_I = \frac{CP}{1+CP} \tag{5.8}$$

Let

$$p_r = \frac{p_2}{p_1} \tag{5.9}$$

and

$$c_r = \frac{c_2}{c_1} \tag{5.10}$$

Then by applying the triangle inequality,

$$|S_{21}| \geq |T_I| \frac{|p_r|}{1+|c_r p_r|} \tag{5.11}$$

and

$$|S_{12}| \geq |T_I| \frac{\frac{1}{|p_r|}}{1+\frac{1}{|c_r p_r|}} \tag{5.12}$$

The equality holds if and only if $c_r p_r$ is real, i.e. $c_r = \alpha \bar{p}_r$, where α is a real number. It can be shown by comparing the two off-diagonal terms of S_o that

$max(|S_{21}|, |S_{12}|)$ is lower bounded by $|T_I|\frac{|p_r|}{1+|p_r|^2}$, and the lower bound can be achieved if and only if α=1. End of proof.

More properties about SITO systems can be found in Freudenberg and Middleton(8), where the "alignment angle" is defined as

$$\phi(j\omega) = arccos(\frac{|C(j\omega)P(j\omega)|}{||C(j\omega)||.||P(j\omega)||}) \tag{5.13}$$

assuming that $P(j\omega)\neq 0$ and $C(j\omega)\neq 0$. The extent to which the two system outputs interact with each other can be quantified by using the alignment angle. It can be shown that $\phi(j\omega) = 0$ if and only if $\frac{c_2(j\omega)}{c_1(j\omega)} = conj(\frac{p_2(j\omega)}{p_1(j\omega)})$. Therefore, the lower bound as described in the above theorem is achieved if and only if the alignment angle is 0.

5.4 Proposed Controller Design Procedure

Based on the theorem described in the previous section, the proposed controller design procedure is as follows.

1. Determine a stable transfer function $W(s)$ which is the best approximation of $conj(\frac{p_1(j\omega)}{p_2(j\omega)})$, and define $c_1(s) = W(s)c_2(s)$. This will guarantee that the interactions between the system outputs as described in the previous section can be minimized.

2. Write $c_1(s)$ in terms of $c_2(s)$, absorb $W(s)$ into the plant, and convert the problem into a typical design problem for a SISO plant searching for c_2.

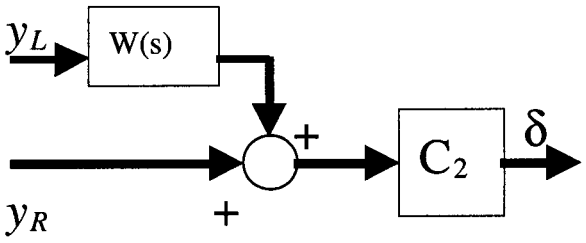

Figure 5.3: Formulation of controller

3. Choose suitable weighting functions, and apply conventional design techniques to find c_2, which minimizes the effects of the system disturbances on the regulated signals, such as lateral deviation and control input.

4. After c_2 is found, the controller C is formulated as shown in Fig.5.3.

Utilizing the parameter values in Table 2.1, $p_1(s)$ and $p_2(s)$ become

$$p_1(s) = \frac{536s^2 + 30720s + 18199}{s^4 + 75s^3 + 1135s^2} \tag{5.14}$$

$$p_2(s) = \frac{-41s^2 - 2454s + 18199}{s^4 + 75s^3 + 1135s^2} \tag{5.15}$$

The frequency responses of $p_1(s)$ and $p_2(s)$ are shown in Fig.5.4 and Fig.5.5. The weighting function is chosen to be

$$W(s) = \frac{-41s^2 - 2454s + 18199}{536s^2 + 30720s + 18199} \tag{5.16}$$

which implies that $conj(\frac{p_2(j\omega)}{p_1(j\omega)})$ is approximated by $\frac{p_2(j\omega)}{p_1(j\omega)}$. This approximation is valid at low frequencies as shown in Fig.5.6. The controller c_2 in step 3 has been

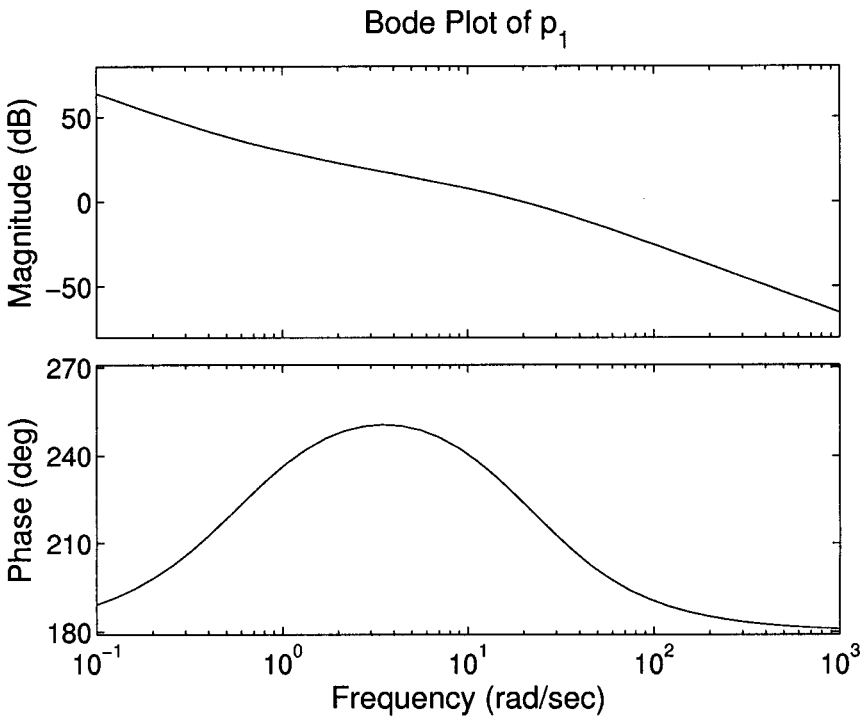

Figure 5.4: Bode plot of $p_1(s)$

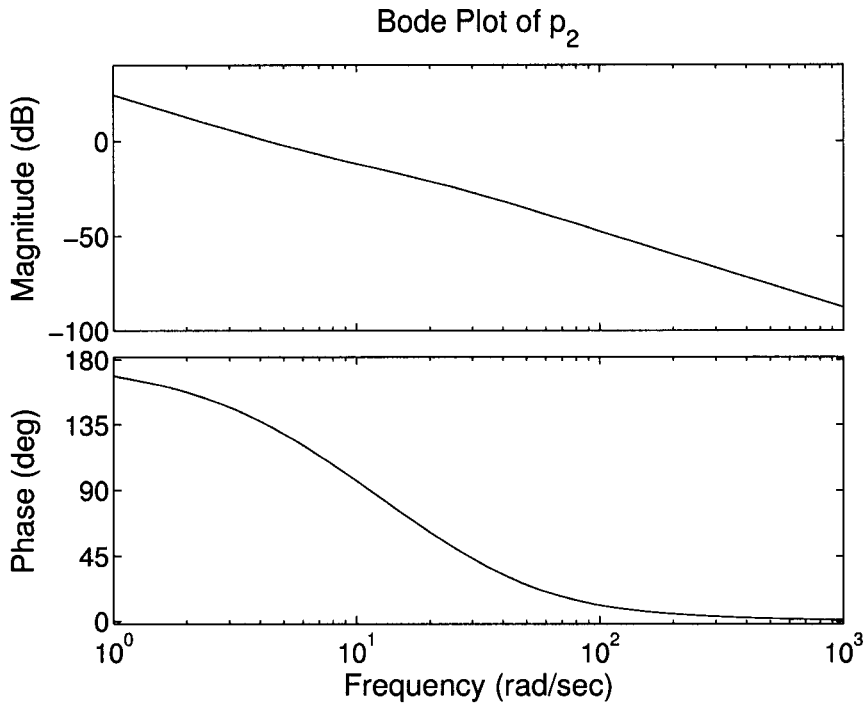

Figure 5.5: Bode plot of $p_2(s)$

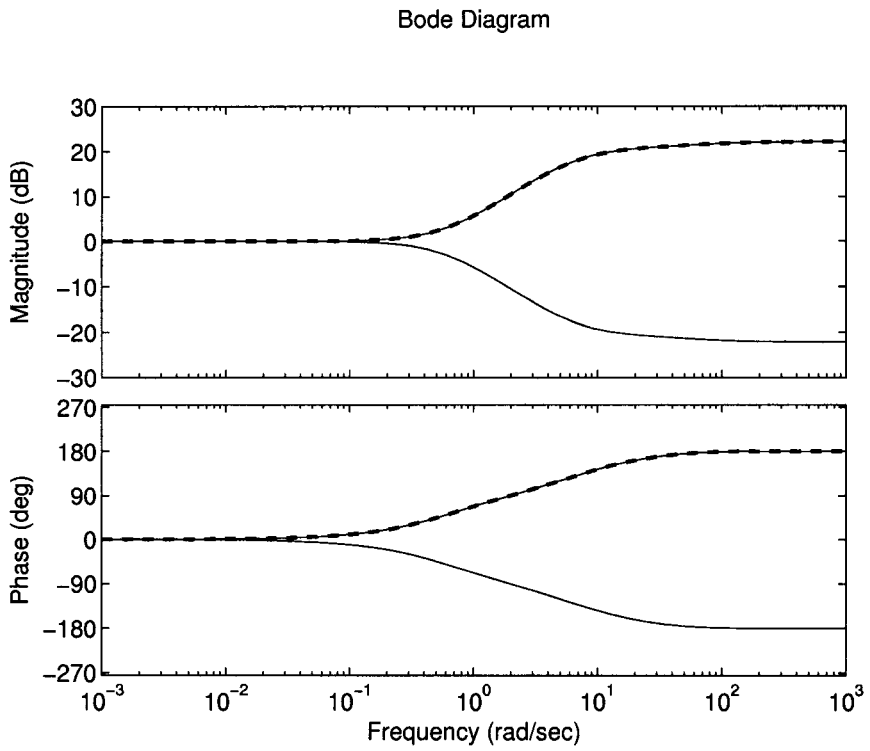

Figure 5.6: Frequency response of $W(j\omega)$ (solid) and $conj\{\frac{p_2(j\omega)}{p_1(j\omega)}\}$ (dashed)

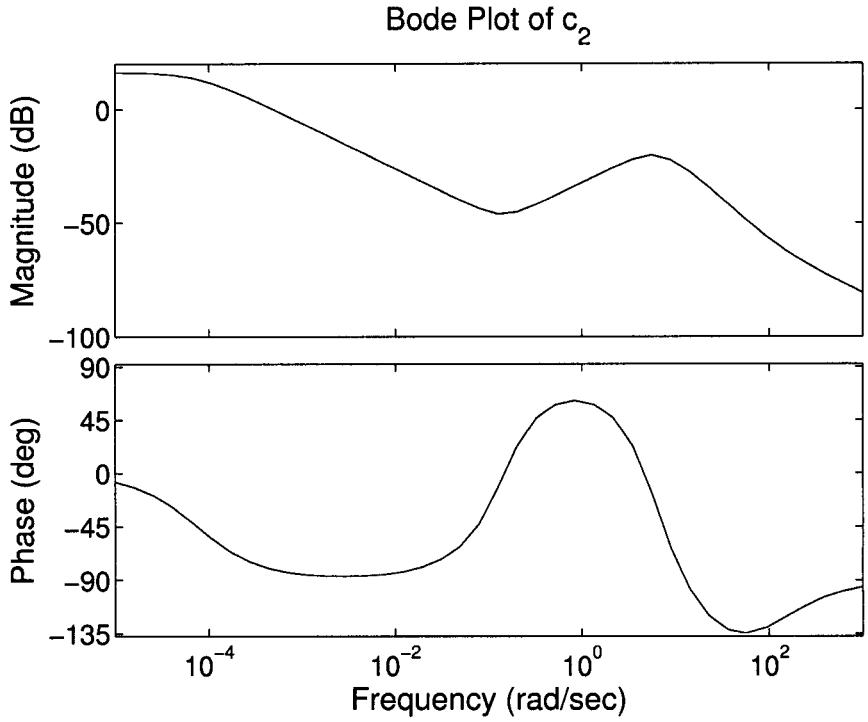

Figure 5.7: Frequency response of $c_2(s)$

designed by using H_∞ techniques and is shown as follows.

$$c_2(s) = \frac{0.09115s^8 + 23.03s^7 + 1953s^6 + 66476s^5 + 756354s^4 + 574700s^3 + 101610s^2 + 8802s + 25}{s^9 + 152s^8 + 8298s^7 + 197922s^6 + 2242627s^5 + 12591485s^4 + 35914851s^3 + 17328941s^2 + 52962s + 3.897} \quad (5.17)$$

The TISO controller can be constructed using c_2 and $W(s)$ as shown in step 4. The frequency responses of c_2 and c_1 are shown in Fig.5.7 and 5.8 respectively. The alignment angle shown in Fig.5.9 is kept small at low frequencies.

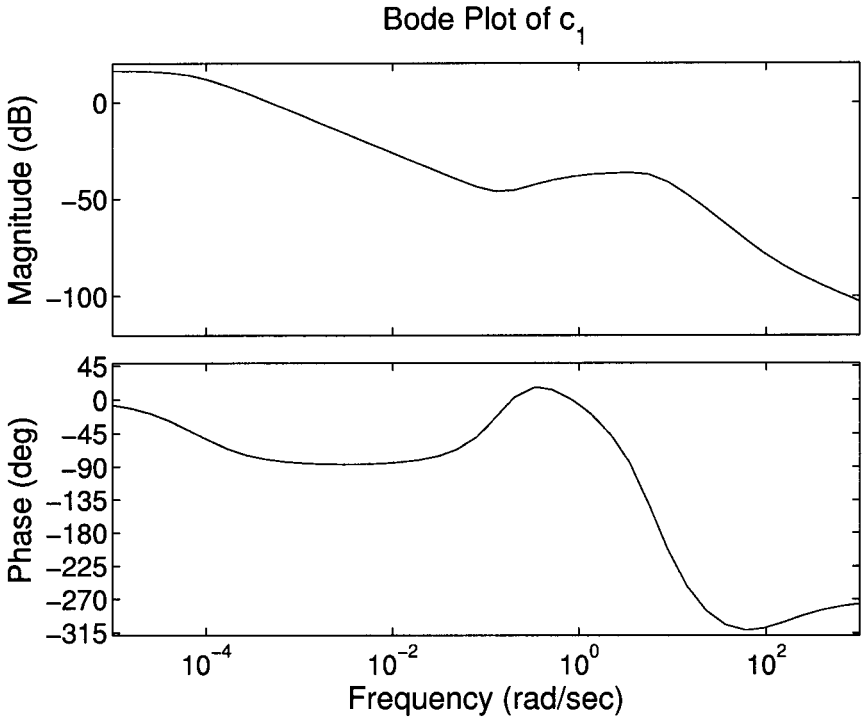

Figure 5.8: Frequency response of $c_1(s)$

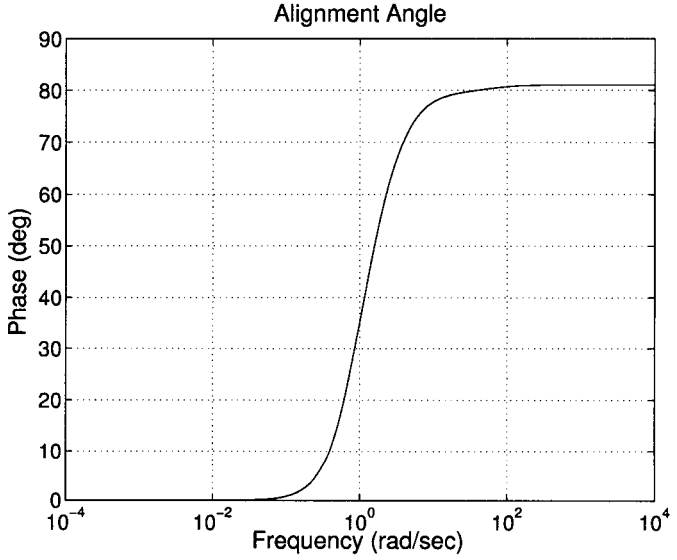

Figure 5.9: Alignment angle

5.5 Simulation Results

Simulations have been conducted on a platoon of four vehicles. The lead vehicle was under normal magnetometer-based control with two sets of magnetometers, and the three following vehicles were under the control algorithm described in the previous section, i.e., each of them utilized measurements from the LIDAR sensor and rear magnetometers, pretending that the front magnetometers had failed. The longitudinal velocity used in the simulation increased from 20 m/s to 40 m/s and remained constant thereafter, as shown in Fig.5.10. Figure 5.11 shows the road curvature profile in the simulations. The simulated road consists of two curved sections, each having a constant road curvature of $\pm 1/800$ [1/m]. Figure 5.12 shows the simulation results. It is evident in the figure that the lateral deviation of each following vehicle is less than that of its preceding vehicle, although the three following vehicles were using exactly the same controller. It should be noted that the tracking performance would have been severely impaired if the feedback system had been obtained solely from the rear magnetometers.

5.6 Experimental Results

The weighting function and the 9th-order controller have been implemented and successfully tested on the same platoon of the two Buick vehicles on the same test track as in the previous testing in Chapter 4. The front vehicle was under

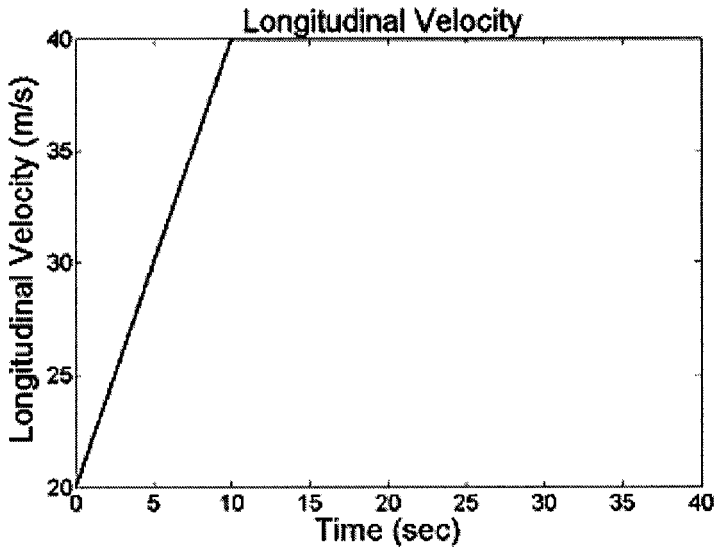

Figure 5.10: Longitudinal velocity profile

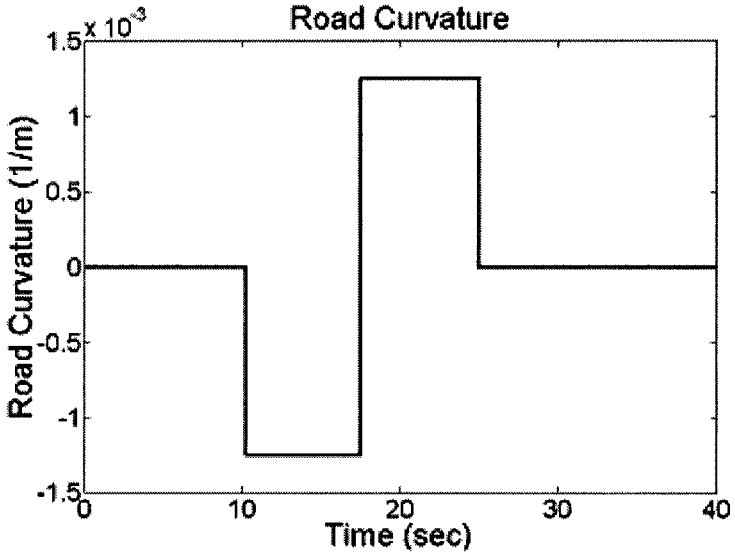

Figure 5.11: Road curvature profile

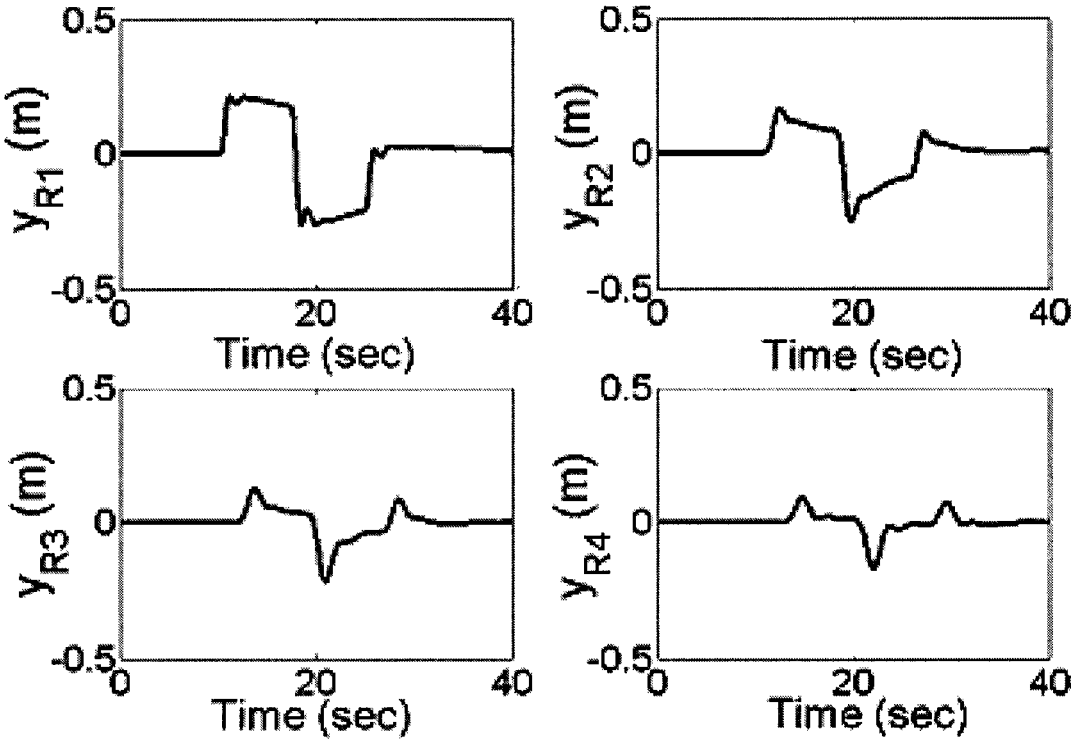

Figure 5.12: Lateral deviation of 4 vehicles in a platoon (y_{Ri} denotes the lateral deviation of the i th vehicle in the platoon measured by the rear magnetometers)

automatic lateral control based on both the front and rear sets of magnetometers. In order to study the effects of different biases in the tracking error of the leading vehicle on that of the following vehicle, two different experiments were conducted, in which the leading vehicle used the same two controllers as described in Chapter 4 respectively (the two magnetometer-based controllers which generated biases in opposite signs when string stability being studied in experiments). The following vehicle was controlled by the proposed 9th-order controller with combined use of LIDAR and rear magnetometer measurements in both experiments. The testing speed was up to 20MPH, and the distance between the two cars was manually maintained at about $10m$. The experimental results when the tracking error of the leading vehicle has a negative bias are shown in Fig.5.13. The experimental results of the lead vehicle are similar to Fig.4.7 since the lead vehicle was under the same controller as in the previous test, and hence are not shown here. The relative lateral and longitudinal position of the controlled vehicle with respect to the lead vehicle were measured by the LIDAR sensor, and the position of the controlled vehicle with respect to the road centerline was measured by the rear magnetometer. The results show that by following both the lead vehicle and road centerline (with combined use of LIDAR and rear magnetometers), the controlled vehicle followed the road centerline with the maximum lateral error of about 35cm. The controller did not work well at the end of the test track, when the road curvature became over 0.008 $[1/m]$, which was not realistic for normal highways. The tracking error

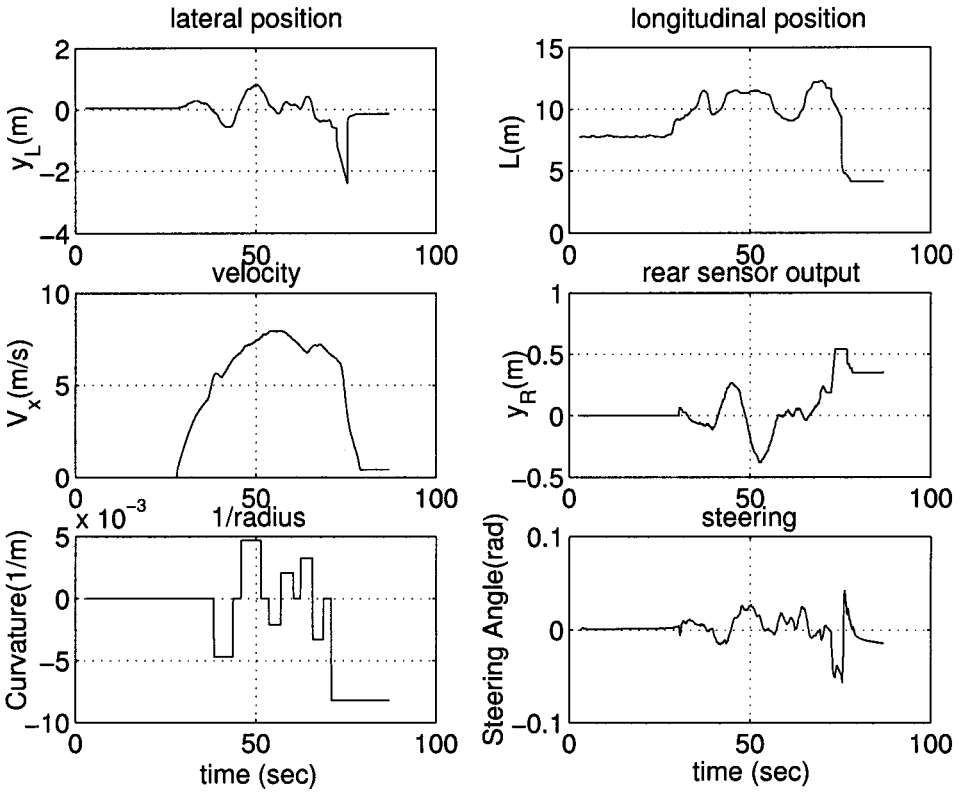

Figure 5.13: Experimental results of following vehicle with combined use of LIDAR and rear magnetometers when the tracking error of the leading vehicle has a negative bias: lateral and longitudinal distance measured by LIDAR sensor, vehicle velocity, rear magnetometer measurements, road curvature, and steering command

of this controller is less than that of the controller using just LIDAR in Chapter 4, since now the vehicle can "see" its deviation from the road centerline through the magnetometers, although they are mounted at the rear end.

The experimental results when the tracking error of the leading vehicle has a positive bias are shown in Figs.5.14 and 5.15. The tracking error of the leading vehicle was smaller than that in the previous testing, and this also resulted in smaller tracking error of the following vehicle. Recall that the two control laws of the leading vehicle generate opposite biases in the tracking error, the results show that the integrated control scheme has effectively reduced the magnification effects of the bias on the following vehicle.

It should be noted that the tracking performance would have been severely impaired if the feedback system had been obtained solely from the rear magnetometers as shown in Fig.5.16. In this case, the controller calculates the required steering angle at the front tires by using only the measurements of the tracking error at the rear end of the car. This makes the rear-magnetometer-based steering control more challenging, especially when the vehicle runs on a curved track. Adjustment of the steering angle can be made only after the vehicle enters or even after it passes the curve. This is the main reason for the oscillations shown in Fig.5.16. However, the oscillations disappear in Fig.5.13, when the controller combines the use of the rear magnetometers with LIDAR, which provides necessary look-ahead information.

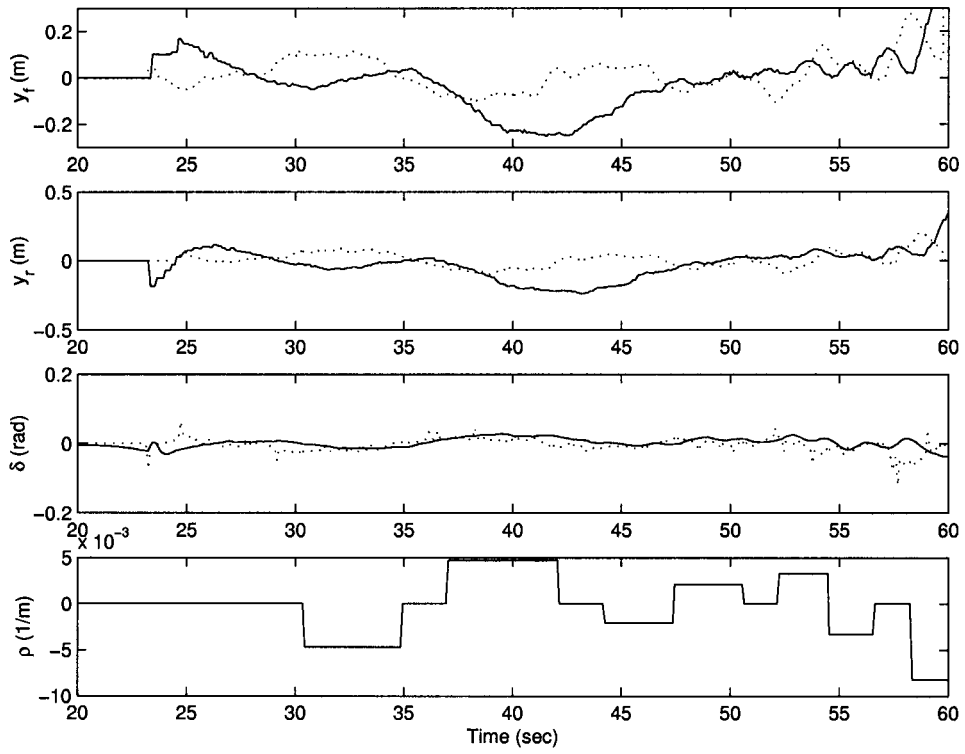

Figure 5.14: Experimental results of following vehicle with combined use of LIDAR and rear magnetometers when the tracking error of the leading vehicle has a positive bias: front, rear magnetometer outputs, steering angle, and road curvature. (solid: following vehicle; dashed: lead vehicle)

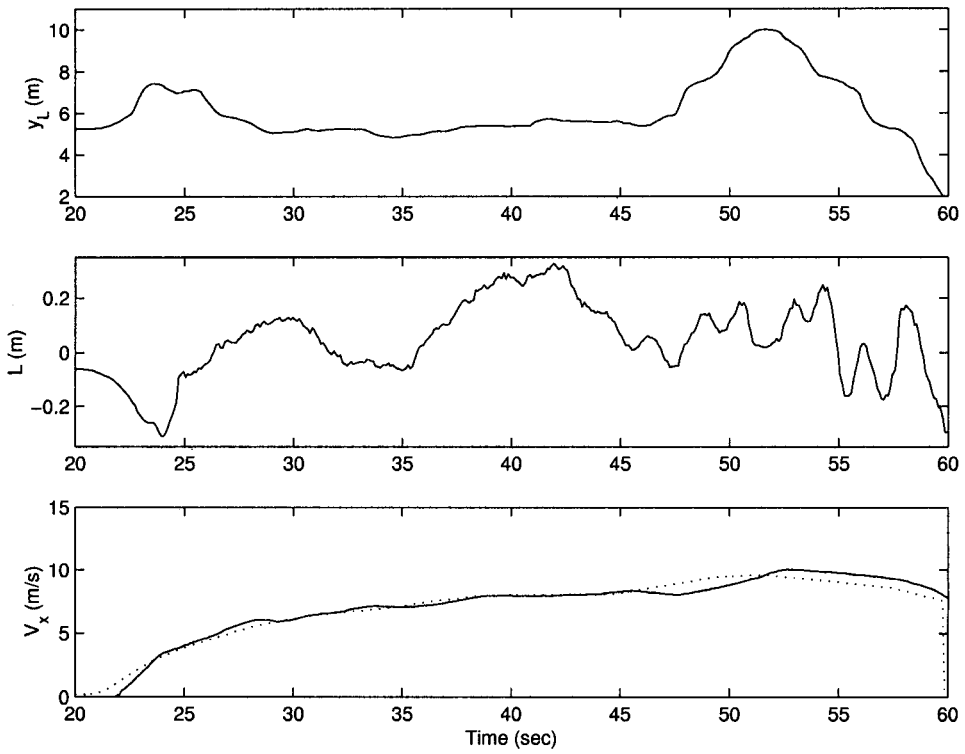

Figure 5.15: Experimental results of following vehicle with combined use of LIDAR and rear magnetometers when the tracking error of the leading vehicle has a positive bias: lateral, longitudinal distance between the two test vehicles measured by LIDAR, and vehicle speed (solid: following vehicle; dashed: lead vehicle)

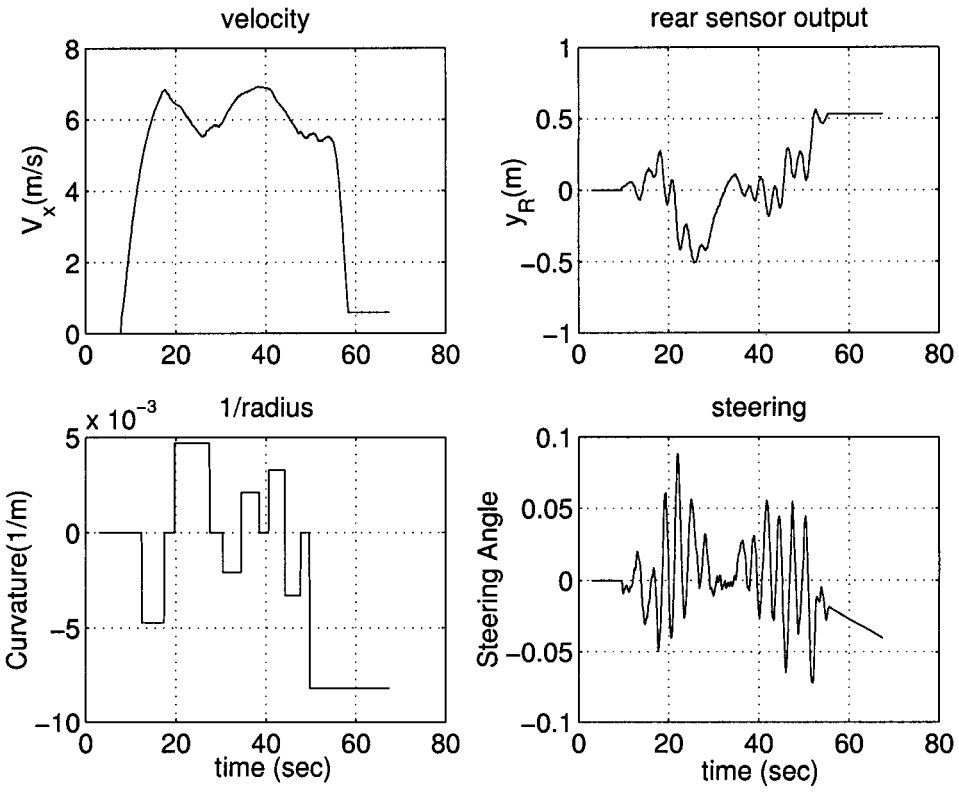

Figure 5.16: Experimental results of vehicle control using just rear magnetometers: vehicle velocity, rear magnetometer measurements, road curvature, and steering command

5.7 Summary

This chapter described the integrated steering control system that combined the LIDAR sensor and magnetometers. This is a mixture of autonomous vehicle following and the magnetometer-based road following approaches. The system may work as a backup system that deals with the partial failure of the on-board magnetometers. Especially this chapter considered the case of front magnetometers failure. The case of rear magnetometer failure is relatively easy to handle since the vehicle lateral dynamics define a minimum-phase system, and has not been discussed in this chapter. The controller design procedure is based on the minimization of the interactions of a single input, two output dynamic system for vehicle lateral control with combined use of the LIDAR sensor and the rear magnetometers. The design procedure guarantees good alignment of the plant and the controller within the closed loop bandwidth, ensuring no strong interactions in the closed loop system, i.e. the unknown actual position and dynamics of the preceding vehicle have little effects on the vehicle lane keeping performance. Two real-time testings have been conducted, in which the leading vehicle was controlled by the two different control algorithms respectively as used in the previous chapter. The two control laws generated small bias in the tracking error of the leading vehicle with opposite signs, but the results show that the integrated control system effectively reduced the bias in the tracking errors of the following vehicle.

Chapter 6

Conclusions and Future Work

6.1 Conclusions

A new approach for vehicle steering control, i.e. autonomous vehicle following, has been studied in this dissertation. In this approach, a vehicle is automatically steered to follow its preceding vehicle. If the leading vehicle is running on the desired track, with small tracking errors, then the following vehicle may also achieve the lane-keeping control goal. This is an indirect lane-keeping control scheme, in the sense that the feedback signals of the closed-loop control system are not relative to the road centerline, but relative to another vehicle. The main benefit of this approach is that it does not rely on any road infrastructure, e.g. lane markers or magnetic markers, hence the system is easy to implement. It may work as an independent driver assistant system, or be combined with a cruise control

system to achieve full automated control of a vehicle. The autonomous vehicle following approach has been studied in recent years(23)(10)(11)(9)(31). The main contributions of this dissertation include analytical and experimental study of the error propagation problem and use of inter-vehicle communication as a solution, integrated control with combined use of vehicle following and road following methods, and a probabilistic association based approach for sensor data processing.

The most significant challenge in developing autonomous vehicle following controllers is the inter-connected feature built in this scheme. The existence of a leading vehicle is required, and the following vehicle can only follow the trajectory of the leading vehicle. This constraint may not be a problem for vehicles which run in platoons, e.g. groups of commercial heavy trucks having the same destination or passenger cars who are willing to run in groups. However, the tracking performance of the following vehicles largely depends on that of the leading vehicle because of the inter-connected feature. The tracking error of the leading vehicle is always transmitted to the following vehicles, and in general the tracking performance of the following vehicles becomes even worse. As the number of vehicles in the platoon increases, the tracking error of the very last vehicle may be unacceptably large. Because all vehicles are inter-connected, the stability of a single vehicle cannot guarantee the stability of the whole platoon. Hence analysis of the string stability problem becomes inevitable. The string stability problem may be solved in two ways. First, if the leading vehicle is equipped with some road following

sensors, e.g. vision sensors, magnetometers, or GPS, communication of the measurements of these sensors to the following vehicles may help reduce the tracking errors of the following vehicles. Second, if all vehicles in the platoon has some kind of road following sensors, even if their measurements are not good enough to enable an effective road following system, the string stability problem may still be solved by incorporating these sensor outputs into the autonomous vehicle following system. Essentially, both methods weaken the coupling between every two adjacent vehicles so that the inter-connected feature in autonomous vehicle following can be removed.

It is still hard to conclude that the autonomous vehicle following scheme can replace road following algorithms, because of the above considerations. Autonomous vehicle following, however, can definitely become helpful to the road following algorithms when some of the road following sensors fail. This dissertation considered magnetometer-based road following systems in the case when one set of the magnetometers have failed. Especially, the more challenging case of front magnetometer failure was considered. Steering control with only the rear magnetometers is hard to realize because the input-output dynamics define a non-minimum phase plant. A back-up control system has been developed to combine the use of LIDAR with rear magnetometers to deal with the case of front magnetometer failure. The controller design principle was based on the minimization of the interactions of a single input, two output dynamic system for closed-loop

vehicle lateral control with combined use of the LIDAR sensor and the rear magnetometers. The design procedure guaranteed good alignment of the plant and the controller within the closed loop bandwidth, ensuring no strong interactions in the closed loop system, i.e. the unknown actual position and dynamics of the preceding vehicle have little effects on the vehicle lane keeping performance. In general, such a solution may also become useful in dealing with other control problems, where two independent sensors are used, but interaction in the closed loop is of major concern.

Another aspect in dealing with multiple sensor outputs was the probabilistic data association method described in Chapter 3. When the LIDAR is used to detect the relative distance between the two vehicles, it emits laser beams to scan in the horizontal plane. The sensor then returns a measurement whenever the laser beams hit a reflective object, which could be the leading vehicle or any other unknown object in the environment. This results in multiple measurements in every sampling period. The probabilistic data association method combines all the measurements according to their probabilities of being the correct measurements, and it constitutes a successful algorithm for tracking the leading vehicle in real time.

6.2 Future Work

One future research topic may be to study the effects of the variation in longitudinal distance on the autonomous vehicle following control performance. Furthermore, future research may be conducted on the integration of LIDAR-based longitudinal control (adaptive cruise control) with autonomous vehicle following.

Due to the limited experimental equipment, experimental validation has only been conducted on two test vehicles. This is not adequate to study the string stability problem in real-time testing. Hence testing with more vehicles may become another research topic. The inter-vehicle communication based approach described in this dissertation communicated magnetometer measurements between the two test vehicles. Future research may be to set up a different communication process for transmitting steering angle command from the leading vehicle to the following vehicles, in which the communicated information will become a feed forward signal to the following vehicle. To achieve this, the steering actuators of the vehicles involved have to be carefully calibrated. This may be done through either hardware work or some intelligent algorithm to be carried out in real time.

Sensor fusion from different types of sensors, sensor arrays, and sensor networks may also be a future research topic. The algorithms presented in this dissertation may be extended in this regard. One direction is to continue to use data association based approach to combine the measurements from different sensors for robust sensing. Another direction is to extend the algorithm described in Chap-

ter 5, with further development for multi-input-multi-output linear or nonlinear systems.

Bibliography

[1] Y. Bar-Shalom. "Tracking Methods in a Multitarget Environment". *IEEE Transactions on Automatic Control*, AC-23(4), 1978.

[2] Y. Bar-Shalom and T. E. Fortmann. *Tracking and Data Association.* Academic Press, Inc., New York, NY, 1988.

[3] Y. Bar-Shalom and A. Jaffer. "Adaptive Nonlinear Filtering for Tracking with Measurements of Uncertain Origin". In *Proceedings of the 1972 IEEE Conference on Decision and Control*, pages 243–247, New Orleans, LA, 1972.

[4] Y. Bar-Shalom and E. Tse. "Tracking in a Cluttered Environment With Probabilistic Data Association". *Automatica*, 11:451–460, 1975.

[5] M. Bertozzi and A. Broggi. "Vision-based Vehicle Guidance". *Computer*, 30(7):49–55, 1997.

[6] C. Chen. *Backstepping Design of Nonlinear Control Systems and Its Application to Vehicle Lateral Control in Automated Highway Systems.* PhD thesis,

Department of Mechanical Engineering, University of California, Berkeley, 1996.

[7] C. Chen and M. Tomizuka. "Dynamic Modeling of Articulated Vehicles for Automated Highway Systems". In *Proceedings of American Control Conference*, pages 653–657, Seattle, WA, 1995.

[8] J. Freudenberg and R. Middleton. "Properties of Single Input, Two Output Feedback Systems". *International Journal of Control*, 72(16):1446–1465, 1999.

[9] H. Fritz. "Longitudinal and Lateral control of Heavy Duty Trucks for Automated Vehicle Following in Mixed Traffic: Experimental Results from the CHAUFFEUR Project". In *Proceedings of the 1999 IEEE International Conference on Control Applications*, Kohala Coast-Island of Hawai'i, Hawai'i, 1999.

[10] T. Fujioka and M. Omae. "Vehicle Following Control in Lateral Direction for Platooning". *Vehicle System Dynamics Supplement*, 28:422–437, 1998.

[11] S. Gehrig and F. Stein. "A Trajectory-Based Approach for the Lateral Control of Car Following Systems". In *Proceedings of the Intelligent Vehicles Symposium '98*, pages 3596–3601, 1998.

[12] J. Goldbeck, B. Huertgen, S. Ernst, and L. Kelch. "Lane Following Combining Vision and DGPS". *Image and Vision Computing*, 18:425–433, 2000.

[13] J. Guldner, H-S. Tan, and S. Patwardhan. "Study of Design Directions for Lateral Vehicle Control". In *Proceedings of the 36th Conference on Decision and Control*, San Diego, CA, 1997.

[14] P. Hingwe and M. Tomizuka. "Robust and Gain Scheduled H_∞ Controllers for Lateral Guidance of Passenger Vehicles in AHS". In *Proceedings of the ASME Dynamic Systems and Control Division*, pages 707–713, 1997.

[15] P. Hingwe, J.-Y. Wang, M. Tai, and M. Tomizuka. Lateral control of heavy duty vehicles for automated highway system: Experimental study on a tractor semi-trailer. California PATH Working Paper UCB-ITS-PWP-2000-1, University of California, Berkeley, 2000.

[16] J. Huang, G. Lu, and M. Tomizuka. Vehicle lateral control under fault in front and/or rear sensors. California PATH Working Paper UCB-ITS-PRR-2000-25, University of California, Berkeley, 2000.

[17] J. Kosecha, R. Blasi, C. J. Taylor, and J. Malik. "Vision-based lateral control of vehicles". In *IEEE Conference on Intelligent Transportation Systems*, pages 900–905, New York, NY, 1997.

[18] G. Lu, J. Huang, and M. Tomizuka. Vehicle lateral control under fault in front and/or rear sensors. California PATH Working Paper UCB-ITS-PRR-2003-26, University of California, Berkeley, 2003.

[19] G. Lu and M. Tomizuka. "Integrated Vehicle Lateral Control with Combined Use of a Laser Scanning Radar Sensor and Rear Magnetometers". In *Proceedings of American Control Conference*, Anchorage, AK, 2002.

[20] G. Lu and M. Tomizuka. "A Laser Scanning Radar Based Autonomous Lateral Vehicle Following Control Scheme for Automated Highways". In *Proceedings of American Control Conference*, Denver, CO, 2003.

[21] G. Lu and M. Tomizuka. "A Practical Solution to the String Stability Problem in Autonomous Vehicle Following". In *Proceedings of American Control Conference*, Boston, MA, 2004.

[22] P. Lugner. "The Influence of the Structure of Automobile Models and Tyre Characteristics on the Theoretical Results of Steady-State and Transient Vehicle Performance". In *The Dynamics of Vehicles, Proceedings of the 5th VSD-wnd IUAM Symposium*, Viena, Sustria, 1997.

[23] V.K. Narendran and J.K. Hedrick. "Autonomous Lateral Control of Vehicles in an Automated Highway System". *Vehicle System Dynamics*, 23:307–324, 1994.

[24] I. Papadimitriou, G. Lu, and M. TomizukaLu. "Autonomous Lateral Following Considerations for Automated Platoons". In *IEEE/ASME International Conference on Advanced Intelligent Mechatronics*, Kobe, Japan, 2003.

[25] S. Patwardhan, H-S. Tan, and J. Guldner. "A General Framework for Automatic Steering Control: System Analysis". In *Proceedings of American Control Conference*, Albuquerque, New Mexico, 1997.

[26] H. Peng and Tomizuka. Lateral control of front-wheel steering rubber-tire vehicles. California PATH Working Paper UCB-ITS-PRR-90-5, University of California, Berkeley, 1990.

[27] K. A. Redmill. "A Simple Vision System for Lane Keeping". In *IEEE Conference on Intelligent Transportation Systems*, pages 212–17, New York, NY, 1997.

[28] L. Segel. "Theoretical Prediction and Experimental Substantiation of the Response of the Automobile to Steering Control". *Automobile Division, The Institute of Mechanical Engineers*, pages 26–46, 1956.

[29] S. Skogestad and I. Postlethwaite. *Multivariable Feedback Control: Analysis and Design.* John Wiley & Sons Ltd., New York, NY, 1996.

[30] D. Swaroop and J. K. Hedrick. "String Stability of Interconnected Systems". *IEEE Transaction on Automatic Control*, 41(3), 1996.

[31] K. Tamura and Y. Furukawa. "Autonomous Vehicle Control System of ICVS City Pal: Electrical Tow-bar Function". In *Proceedings of the IEEE Intelligent Vehicles Symposium 2000*, Dearborn, MI, 2000.

[32] J.-Y. Wang and M. Tomizuka. "Analysis and Controller Design Based on Linear Model for Heavy-Duty Vehicles". In *International Mechanical Engineering Congress & Exposition, ASME Symposium on Transportation Systems*, pages 729–735, Anaheim, CA, 1998.

[33] J.-Y. Wang and M. Tomizuka. "Dynamics Analysis and Robust Steering Controller Design for Automated Lane Guidance of Heavy-Duty Vehicles". *Asian Journal of Control*, 2(3):140–154, 2000.

[34] R. White and M. Tomizuka. "Autonomous Following Lateral Control of Heavy Vehicles Using Laser Scanning Radar". In *Proceedings of American Control Conference*, Arlington, VA, 2001.

[35] R. White and M. Tomizuka. "Estimating Relative Position and Yaw with Laser Scanning Radar Using Probabilistic Data Association". In *Proceedings of American Control Conference*, Anchorage, AK, 2002.